図4　1才以上症例における外科切除率と予後

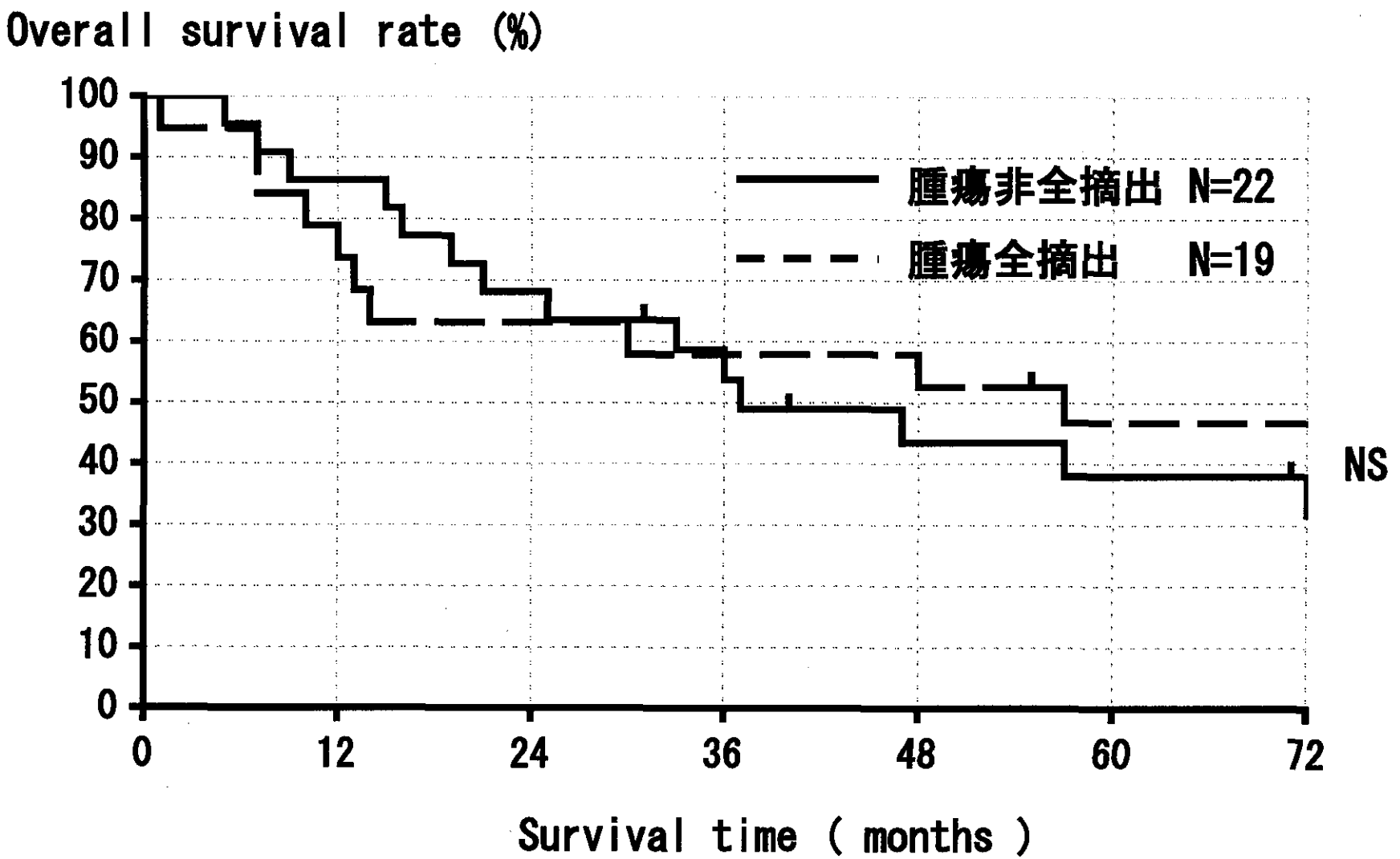

図5　1才以上進行症例における外科切除率と予後

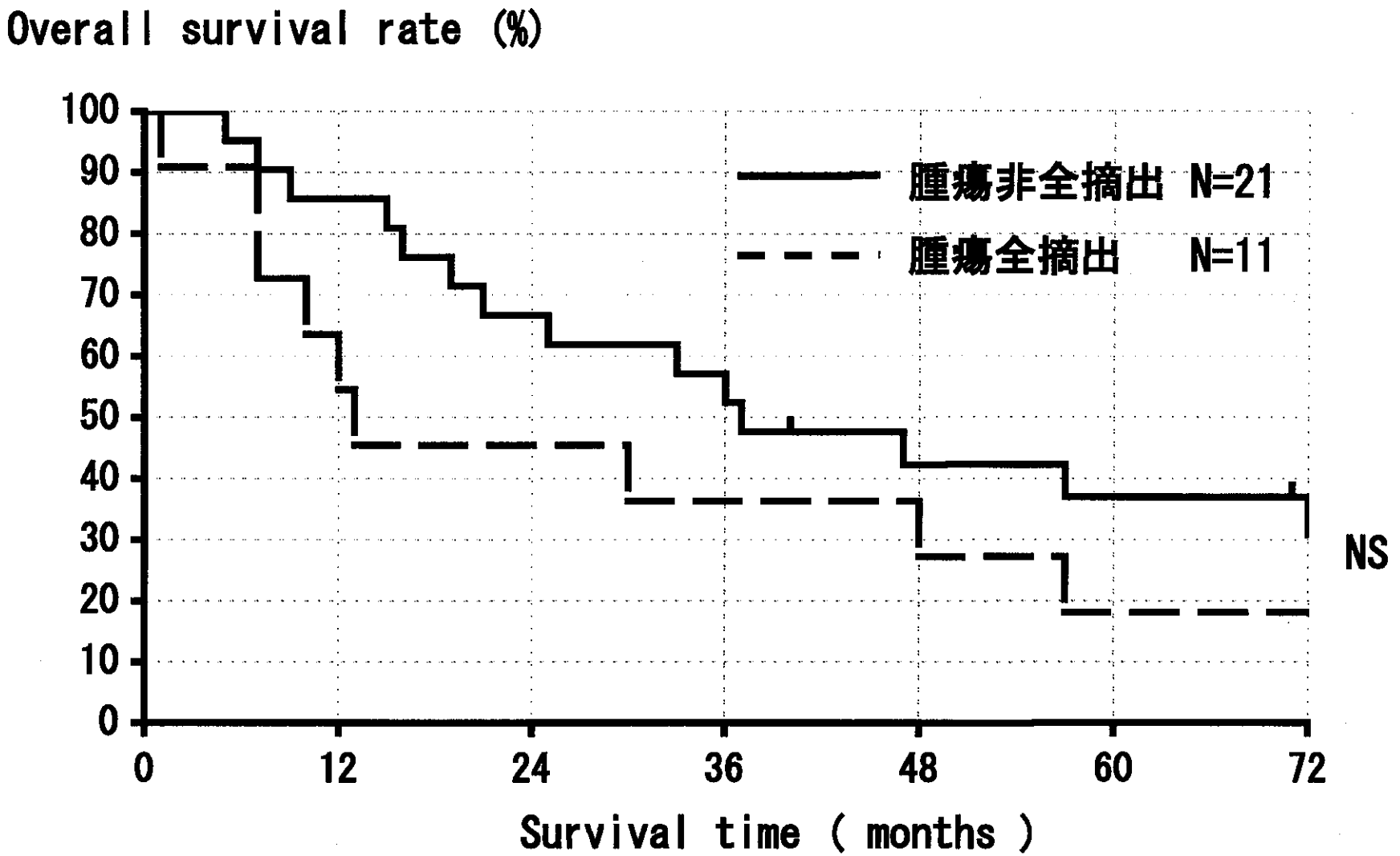

CpG Island Methylator Phenotype Is a Strong Determinant of Poor Prognosis in Neuroblastomas

Masanobu Abe,[1,2] Miki Ohira,[3] Atsushi Kaneda,[1] Yukiko Yagi,[1] Seiichiro Yamamoto,[4] Yoshihiro Kitano,[5] Tsuyoshi Takato,[2] Akira Nakagawara,[3] and Toshikazu Ushijima[1]

[1]Carcinogenesis Division, National Cancer Center Research Institute; [2]Department of Oral and Maxillo Facial Surgery, University of Tokyo Graduate School of Medicine; [3]Biochemistry Division, Chiba Cancer Center Research Institute; [4]Information Division, Research Center for Cancer Prevention and Screening, National Cancer Center; and [5]Department of Pediatric Surgery, National Center for Child Health and Development, Tokyo, Japan

Abstract

Neuroblastoma, one of the most common pediatric solid tumors, is characterized by two extreme disease courses, spontaneous regression and life-threatening progression. Here, we conducted a genome-wide search for differences in DNA methylation that distinguish between neuroblastomas of the two types. Three CpG islands (CGI) and two groups of CGIs were found to be methylated specifically in neuroblastomas with a poor prognosis. By quantitative analysis of 140 independent cases, methylation of all the five CGI (groups) was shown to be closely associated with each other, conforming to the CpG island methylator phenotype (CIMP) concept. The presence of CIMP was sensitively detected by methylation of the *PCDHB* CGIs and associated with significantly poor survival (hazard ratio, 22.1; 95% confidence interval, 5.3-93.4; $P < 0.0001$). Almost all cases with N-*myc* amplification (37 of 38 cases) exhibited CIMP. Even in 102 cases without N-*myc* amplification, the presence of CIMP (30 cases) strongly predicted poor survival (hazard ratio, 12.4; 95% confidence interval, 2.6-58.9; $P = 0.002$). Methylation of *PCDHB* CGIs, located in their gene bodies, did not suppress gene expression or induce histone modifications. However, CIMP was significantly associated with methylation of promoter CGIs of the *RASSF1A* and *BLU* tumor suppressor genes. The results showed that neuroblastomas with CIMP have a poor prognosis and suggested induction of silencing of important genes as an underlying mechanism. (Cancer Res 2005; 65(3): 828-34)

Introduction

Epigenetic abnormalities, especially alterations in DNA methylation, are intimately involved in development of various human tumors (1). Aberrant methylation of promoter CpG islands (CGI) causes inactivation of tumor suppressor genes. Genomic instability is caused by genomic hypomethylation and is associated with hypermethylation (2, 3). Identification of epigenetic abnormalities in human cancers is expected to lead not only to discovery of novel disease mechanisms but also to development of new diagnostic markers. Therefore, we previously developed a genome-wide scanning method, methylation-sensitive representational difference analysis (MS-RDA), for detecting differences in DNA methylation (4, 5). This technique analyzes unmethylated, CpG-rich regions of the genome and has already identified genes silenced in human lung, stomach, breast, and pancreatic cancers (6–9).

Neuroblastoma derived from primitive cells of the sympathetic nervous system is one of the most common solid tumors in childhood, characterized by two extreme disease courses, spontaneous regression, and life-threatening progression (10, 11). The clinical outcome is associated with disease stage, age at diagnosis, histologic classification, N-*myc* amplification, DNA ploidy, and *TrkA* overexpression (10–12). These characteristics are therefore used to classify cases into low-, intermediate-, and high-risk groups. However, especially in the cases with intermediate risk, prediction of prognosis and therapeutic decision-making are still difficult, and development of new markers is an urgent priority. Moreover, the molecular bases underlying the two distinct clinical courses are still unknown, and their clarification is needed to allow development of novel therapeutics.

In the present study, considering the major involvement of epigenetic machinery in embryonic development (13, 14), we searched for differences in DNA methylation between neuroblastomas with a good prognosis and counterparts with a poor prognosis by MS-RDA.

Materials and Methods

Tissue Samples and Cell Lines. Tumor samples were obtained from 145 nonrecurrent cases between 1995 and 1999 and were used under approval of institutional review boards. The mean age at initial diagnosis was 27 months (range, 0-216 months). Their clinical stages were determined according to the International Neuroblastoma Staging System, and 40, 17, 20, 60, and 8 cases belonged to stages I, II, III, IV, and IVS, respectively. Normal adrenal medulla tissue was collected from a case undergoing nephrectomy for a renal cancer. Neuroblastoma cell lines were obtained from the American Type Culture Collection (Manassas, VA), the Japanese Collection of Research Bioresources (Tokyo, Japan), and the RIKEN Bio Resource Center (Tsukuba, Japan). GANB was established by A.N. and normal human bronchial epithelial cells were purchased from Cambrex (East Rutherford, NJ). High molecular weight DNA and total RNA were extracted as previously described (7). Total RNAs of brain and adrenal glands were purchased from Clontech (Palo Alto, CA).

MS-RDA and Database Search. MS-RDA was done as previously described (4, 5). Genomic DNA of primary neuroblastomas with a good prognosis (cases 92, 98, 104, 112, and 148) and neuroblastoma cell lines established from cases with a poor prognosis (CHP134, IMR32, GANB, NGP, and TGW) were digested with *Hpa*II, and then two pooled DNA samples were prepared. Although use of cell lines is highly recommended for MS-RDA (5), no cell lines were available for neuroblastomas with a good prognosis, and therefore we used the primary samples. To isolate CGIs that were hypermethylated in the latter, the cell line pool was used as the tester, and the primary tumor pool as the driver. MS-RDA in the opposite direction

Note: Supplementary data for this article are available at Cancer Research online (http://cancerres.aacrjournals.org/).

Requests for reprints: Toshikazu Ushijima, 5-1-1 Tsukiji, Chuo-ku, Tokyo 104-0045, Japan. Phone: 133-547-5240; Fax: 135-565-1753; E-mail: tushijim@ncc.go.jp.

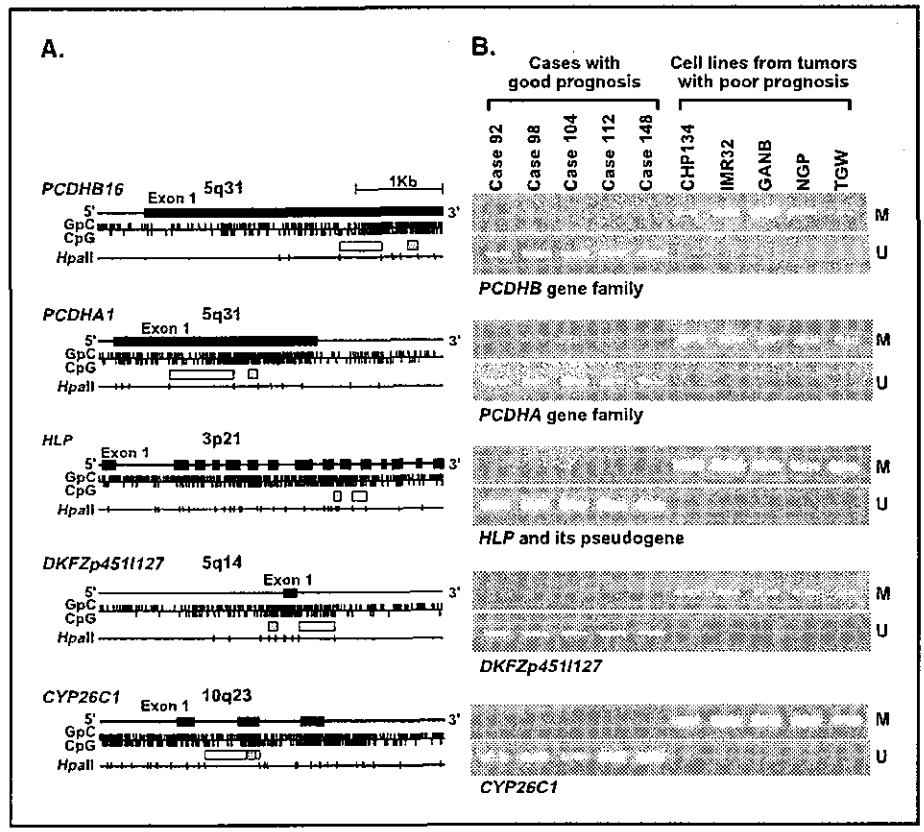

Figure 1. Five CGIs isolated by MS-RDA and their methylation statuses in the samples used for MS-RDA. *A*, genomic structures of the five CGIs. GpC, CpG, and *Hpa*II recognition sites (5′-CCGG-3′) are shown by ticks. *Closed boxes*, exons; *open boxes*, clones isolated by MS-RDA; *shaded boxes*, regions analyzed by MSP. *B*, methylation statuses analyzed by MSP. *M*, MSP using primers specific to methylated DNA; *U*, MSP using primers specific to unmethylated DNA. All the five CGIs were found to be differentially methylated between the two groups used for MS-RDA.

was also done. For each series of MS-RDA, 96 clones were analyzed for redundancy, and nonredundant clones were sequenced. Their genomic origins were examined using BLASTN software http://www.ncbi.nlm.nih.gov/BLAST/).

Sodium Bisulfite Modification and Methylation-Specific PCR. One microgram of DNA underwent sodium bisulfite modification (15), and was suspended in 20 μL of TE buffer. For methylation-specific PCR (MSP), 1 μL of the solution was used for PCR with primers specific to methylated or unmethylated sequences. Using DNA from normal human bronchial epithelial and DNA methylated with *Sss*I methylase, annealing temperatures specific for methylated and unmethylated primers were determined. Quantitative MSP was done separately for methylated DNA molecules and for unmethylated DNA molecules. Standard DNA was prepared by cloning PCR products amplified by methylated and unmethylated primers into a vector, respectively. The numbers of methylated and unmethylated molecules in a test sample were determined by comparing their amplification with those of standard samples containing 10 to 10^6 molecules. The "methylation index" was calculated as the fraction of methylated molecules in the total DNA molecules (no. methylated molecules + no. unmethylated molecules). Each sample was analyzed twice, blind to clinical information, and high reproducibility was confirmed (correlation coefficient = 0.98).

The *protocadherin* β (*PCDHB*) family consists of 16 genes with single exons and three pseudogenes on 5q31, and their CGIs are located in the gene bodies. MSP primers were designed to recognize 17 of the 19 members (all except for the *PCDHB1* gene and the *PCDHB19* pseudogene). The *protocadherin* α (*PCDHA*) family consists of 15 genes and one pseudogene having unique first exons and shared exons 2 to 4 on 5q31, and their CGIs are located in exon 1. MSP primers were designed to recognize 13 of the 16 members (all except for the *PCDHAC1* and *PCDHAC2* genes and the *PCDHA14* pseudogene). The *hepatocyte growth factor-like protein* (*HLP/MSP/MST1*) gene is highly homologous to *macrophage stimulating, pseudogene 9* (*MSTP9*), and MSP primers were designed to recognize both of these. For *DKFZp451I127*, *FLJ37440*, *Zinc finger protein 297* (*ZNF297*), and *Cytochrome p450 CYP26C1* (*CYP26C1*), MSP primers were designed to recognize each of them specifically. The primers and PCR conditions are shown in Supplementary Table 1.

Semiquantitative and Quantitative Reverse Transcription-PCR. cDNA was synthesized from 3 μg of total RNA treated with DNase using a Superscript II kit (Invitrogen Co., Carlsbad, CA). For semiquantitative reverse transcription-PCR (*PCDHB1-PCDHB15*), multiple cycles of PCR were tested for each gene, and numbers giving a wide dynamic range were determined. The primers and PCR conditions are shown in Supplementary Table 2. For quantitative reverse transcription-PCR (*PCDHB16*), the number of cDNA molecules was determined by quantitative PCR, as in quantitative MSP, and the copy number was normalized to that of *GAPDH*.

Chromatin Immunoprecipitation Assay. From 1×10^6 cells, DNA/histone complexes were immunoprecipitated, and DNA was eluted in 30 μL of TE after reversing cross-linking. Copy numbers of DNA molecules of the *PCDHB16* exon, *RASSF1A* promoter, and *GAPDH* promoter in 1 L of the eluate were determined by quantitative PCR (primer sequences in Supplementary Table 3), and normalized to the copy numbers in the input. Anti-acetyl-histone H3 antibody (AcH3) and anti-dimethylated-histone H3 (lysine 9; MetH3K9) were purchased from Cell Signalling (Beverly, MA).

Statistical Analysis. Associations between methylation levels among CGI groups were examined using the Pearson correlation coefficient and Fisher's exact test. Survival time was measured from the date of initial diagnosis to the date of death or last contact. Kaplan-Meier analysis and log-rank tests were done to compare survival between the groups defined by methylation levels. Hazard ratio (HR) between groups and dose-response relationships between methylation levels and survival were estimated by the Cox proportional hazard model. Kaplan-Meier curves were drawn with the help of Aabel software (Gigawiz. Ltd. Co., Tulsa, OK) and other analyses were conducted using SAS version 8.2 (SAS Institute, Inc., Cary, NC).

Results

Genome-Scanning for Differentially Methylated CpG Islands. MS-RDA was done using five primary neuroblastomas with a good prognosis and five neuroblastoma cell lines established from cases with a poor prognosis. Seven DNA fragments, derived from CGIs of *PCDHB16*, *PCDHA1*, *HLP*, *DKFZp451I127*, *FLJ37440*, *ZNF297*, and *CYP26C1*, were isolated as methylated in the latter samples. No DNA fragments were isolated as methylated in the former samples. Methylation statuses of (i) 17 CGIs of the *PCDHB* family (detailed structure in Supplementary Fig. 1), (ii) 13 CGIs of the *PCDHA* family, (iii) *HLP* and its pseudogene, and (iv) other four unique CGIs were examined by MSP. This revealed that the *PCDHB* family (5q31), the *PCDHA* family (5q31), *HLP* (3p21) and its pseudogene (1p36), *DKFZp451I127* (5q14), and *CYP26C1* (10q23) were specifically methylated in the latter samples (Fig. 1*A* and *B*).

Close Association between Methylation and Poor Prognosis in 140 Independent Primary Samples. To analyze the significance of the differential methylation of the above five CGI (groups) in primary neuroblastomas, 140 primary samples, all different from the initial five samples, were analyzed by quantitative MSP. When distributions of methylation indices were analyzed (Fig. 2), a clear bimodal distribution was observed for (i) the CGI group in the *PCDHB* family (17 CGIs), (ii) the CGIs of *HLP* and its pseudogene, and (iii) the *CYP26C1* CGI. The results thus indicated that the cases could be classified into two groups, one with high methylation and the other with low methylation. The dose-response relationships between high *PCDHB* methylation and poor prognosis were analyzed by the Cox proportional model using the methylation index as a continuous value, and the association was confirmed with a trend $P < 0.0001$. Normal adrenal medulla had a methylation index of 4%.

According to the bimodal distribution, the effect of high methylation was assessed by dichotomous groups. For the *PCDHB* family, cutoff values of 30%, 40%, 50%, 60%, 70%, and 80% were tested, and HRs of 16.8 [95% confidence interval (95% CI), 4.0-70.9], 22.1 (95% CI, 5.3-93.4; Fig. 3), 13.1 (95% CI, 4.5-37.9), 9.1 (95% CI, 3.8-23.4), 7.0 (95% CI, 3.1-15.8), and 7.8 (95% CI, 3.4-17.6), respectively, were obtained ($P < 0.001$ for all cutoff values). This showed that cases can be classified into two groups with distinct prognoses, and we adopted a cutoff value of 40%, which gave the highest HR, for convenience in the following analysis.

The dose-response relationships were also confirmed for other four CGI (groups), *PCDHA* ($P = 0.004$), *HLP* ($P < 0.0001$), *DKFZp451I127* ($P = 0.02$), and *CYP26C1* ($P < 0.0001$). Cutoff values were similarly tested, and those for *PCDHA*, *HLP*, *DKFZp451I127*, and *CYP26C1* were set at 80%, 10%, 20%, and 70%, respectively, with HRs of 5.7 (95%CI, 1.4-24.0; $P = 0.07$), 21.7 (95% CI, 5.1-91.4; $P < 0.0001$), 3.2 (95% CI, 1.0-10.5; $P = 0.045$), and 8.7 (95% CI, 4.1-18.1; $P < 0.0001$), respectively (Fig. 3).

Existence of the CpG Island Methylator Phenotype in Neuroblastomas. Methylation of the different CGI (groups) had shown close associations with each other (Table 1). When correlation was analyzed as a continuous value, Pearson correlation coefficients between *PCDHB* and *PCDHA*, *HLP*, *DKFZp451I127* and *CYP26C1* were 0.55, 0.70, 0.26 and 0.77, respectively. This showed that multiple CGIs were simultaneously methylated in

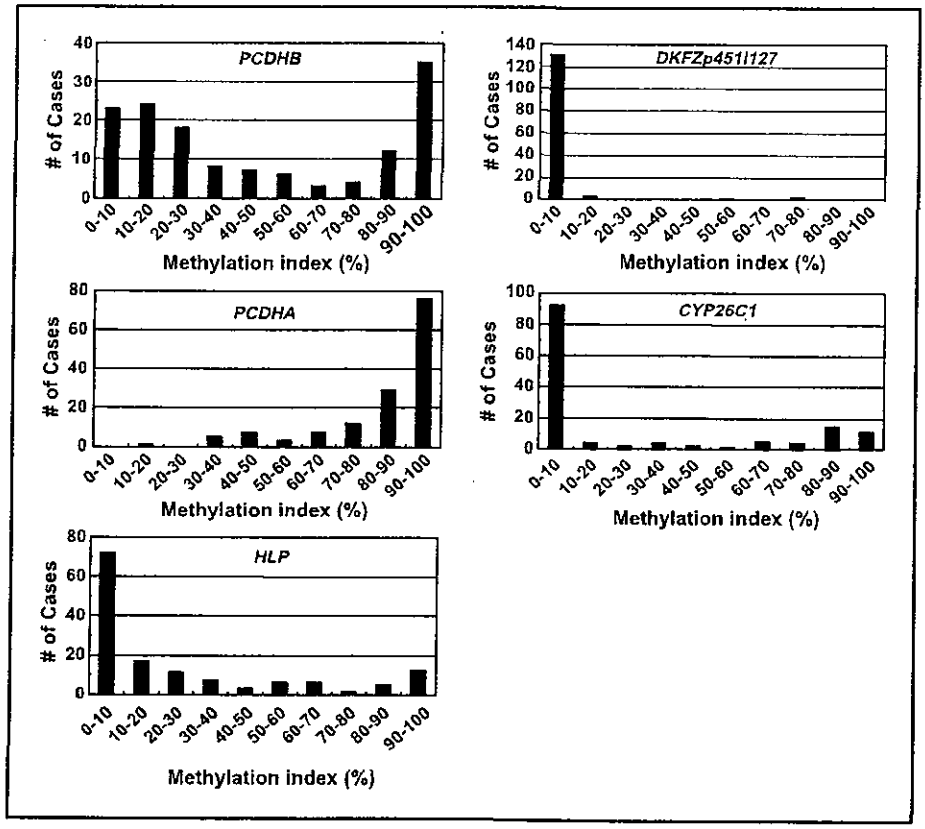

Figure 2. The distribution of methylation indices among the 140 cases analyzed: (*i*) 17 CGIs of the *PCDHB* family, (*ii*) 13 CGIs of the *PCDHA* family, (*iii*) CGIs of *HLP* and its pseudogene, (*iv*) *DKFZp451I127*, and (*v*) *CYP26C1*.

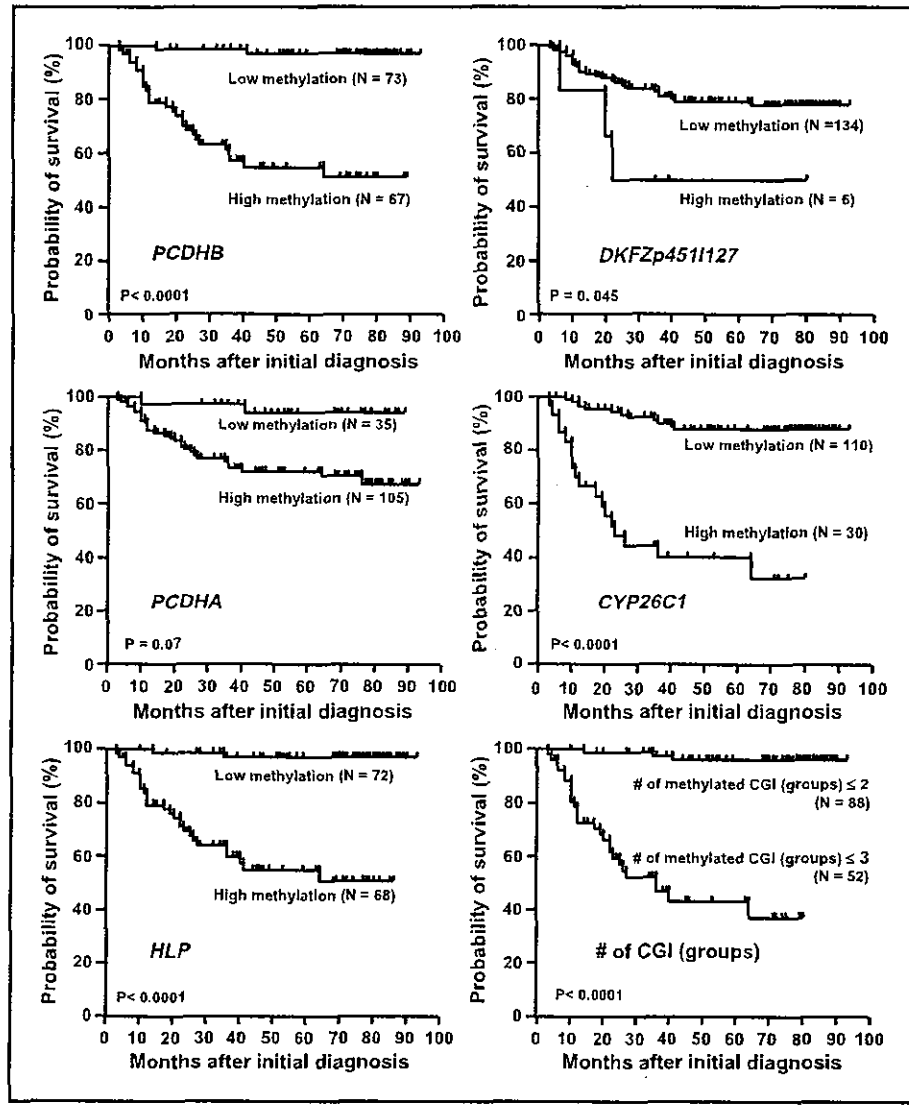

Figure 3. Predictive powers of methylation of the five CGI (groups) identified, and their multiple methylation: (*i*) 17 CGIs of the *PCDHB* family, (*ii*) 13 CGIs of the *PCDHA* family, (*iii*) CGIs of *HLP* and its pseudogene, (*iv*) *DKFZp451I127*, (*v*) *CYP26C1*, and (*vi*) methylation of three of these or more were analyzed by the Kaplan-Meier method using 140 primary samples. The *PCDHB* family, *HLP*, *DKFZp451I127*, *CYP26C1*, and methylation of multiple CGI (groups) had significant influence on survival.

neuroblastomas with a poor prognosis (Supplementary Fig. 2*A*). The simultaneous methylation of (i) 17 CGIs of the *PCDHB* family, (ii) 13 CGIs of the *PCDHA* family, (iii) CGIs of *HLP* and its pseudogene, (iv) *DKFZp451I127* CGI, and (v) *CYP26C1* CGI conformed with the concept of the CpG island methylator phenotype (CIMP; ref. 16).

Associations between CIMP and poor prognosis were examined by defining CIMP as cases with methylation of two CGI (groups) or more, those with three or more, those with four or five, and those with five. When CIMP was defined as cases with methylation of three CGI (groups) or more, the largest association with poor prognosis was observed, with a HR of 25.4 (95% CI, 7.6-84.5; Fig. 3). However, the HR (22.1) given by 17 CGIs of the *PCDHB* gene family approximated to this, and the *PCDHB* methylation level closely correlated with the number of methylated CGI (groups; Supplementary Fig. 2*B*). Therefore, for simplicity of analysis, we defined CIMP in neuroblastomas on the basis of high methylation of the *PCDHB* family, tentatively with a cutoff value of 40%.

Predictive Power of CIMP, Compared with Known Prognostic Factors. Univariate analyses showed that N-*myc* amplification, low *TrkA* expression, DNA diploidy, and an age no younger than 1 year gave HRs of 9.5 (95% CI, 4.4-20.5), 3.9 (95% CI, 1.7-9.3), 4.2 (95% CI, 1.65-10.8), and 12.3 (95% CI, 3.7-41.7). Cases were stratified by these known factors (Table 2). In those without N-*myc* amplification, CIMP also showed an influence with a HR of 12.4 (95% CI, 2.6-58.9), but almost all cases with N-*myc* amplification (37 of the 38 cases) showed CIMP. It was suggested that cases with N-*myc* amplification were contained in the cases with CIMP. CIMP was independent from *TrkA* overexpression, DNA ploidy, and age at diagnosis. Stage seemed to be a stronger prognostic factor. Notably, even when limited to cases in stages III and IV without N-*myc* amplification, which are classified into the intermediate risk group and clinically important, CIMP gave a HR of 4.8 (95% CI, 1.0-23.0; $P = 0.048$).

Multivariate analyses were finally done taking all the five known prognostic factors into account. Although CIMP gave a HR of 5.0 (95% CI, 0.47-52.7), it was not significant ($P = 0.18$), possibly due to limitation in the number of cases.

Table 1. Association between the *PCDHB* methylation and methylation of other CGIs

Variables	Methylation level of *PCDHB* family gene		*P**
	High (≥40%)	Low (<40%)	
No. cases (n = 140)	67	73	
Methylation of CGIs outside promoter regions (n = 140)			
PCDHA gene family (exon 1)†	65/67	41/73	<0.0001
HLP (exons 2-13)‡	52/67	16/73	<0.0001
CYP26C1 (exon 2)§	30/67	0/73	<0.0001
p41Arc (intron 8)	1/67	1/73	0.48
SIM2 (exon 2)	0/67	0/73	
Methylation of CGIs in promoter regions (n = 140)			
DKFZp451I127‖	6/67	0/73	0.011
RASSF1A	51/67	10/73	<0.0001
BLU	25/67	3/73	<0.0001
p16	0/67	0/73	
hMLH1	0/67	0/73	
PCDHB1	0/67	0/73	
TAF7	0/67	0/73	
p41Arc	0/67	0/73	
SIM2	0/67	0/73	

*Fisher's exact test.
†Boundaries for high methylation and low methylation of *PCDHA* gene family were set at 80% of the methylation index.
‡Boundaries for high methylation and low methylation of *HLP* were set at 10% of the methylation index.
§Boundaries for high methylation and low methylation of *CYP26C1* were set at 70% of the methylation index.
‖Boundaries for high methylation and low methylation of *DKFZp451I127* were set at 20% of the methylation index.

Effects of PCDHB Methylation on Gene Expression and Chromatin Structure. The CGIs of the *PCDHB* family were located in their gene bodies, whose methylation generally does not block gene transcription (17). The actual effects of methylation on expression were examined for 16 genes of the *PCDHB* family using 10 primary neuroblastomas with low methylation and five primary neuroblastomas with high methylation. The methylation was not associated with loss of expression (*a representative result* is shown in Fig. 4*A*). The effect of methylation of the *PCDHB16* CGI on the histone modification was further examined by chromatin immunoprecipitation assay. It was found that DNA methylation of the *PCDHB16* CGI did not induce histone H3 lysine 9 methylation or histone H3 deacetylation (data not shown).

Association between CIMP and Promoter Methylation. High methylation of *PCDHB* CGIs, a sensitive surrogate marker of CIMP in neuroblastomas, did not repress gene expression or induce histone modification. This indicated that CIMP is involved in the poor prognosis of neuroblastomas by causing methylation of promoter CGIs, although it is known that promoter CGIs are resistant to *de novo* methylation (18, 19).

Among the five CGI (groups) identified in this study, only that of *DKFZp451I127* was located in a promoter region. Although its methylation was infrequent, the methylation was observed only in neuroblastomas with CIMP (Table 1), and was associated with expression loss (Fig. 4*B*). To make the association clearer, methylation statuses were analyzed for eight additional CGIs in promoter regions. It was shown that methylation of promoter CGIs of *RASSF1A* (3p21) and *BLU* (3p21) was far more frequently observed in neuroblastomas with CIMP (Table 1, $P < 0.0001$). At the same time, there was a preference for CGIs affected by CIMP among CGIs in promoter regions, and also among those outside promoter regions (Table 2).

Discussion

Extensive methylation of multiple CGIs, conforming with the concept of CIMP, was here found specifically present in neuroblastomas with a poor prognosis and could be sensitively detected by focusing on the *PCDHB* family. *PCDHB* methylation did not suppress gene expression or induce histone modification. However, CIMP was associated with promoter methylation of *RASSF1A* and *BLU* genes and one of the mechanisms underlying the poor prognosis of neuroblastomas seemed to be silencing of these and possibly other tumor suppressor genes and genes important for differentiation.

CIMP was originally identified in colon cancers (16), but there has been some dispute over its presence (20). The clear correlation between CIMP and a poor prognosis found here for neuroblastomas was unequivocal and presumably reflects an intrinsic tendency for methylation of CGIs. This is because, first, neuroblastomas have a much shorter history than colon cancers, and the accumulated number of methylated CGIs in neuroblastomas is expected to parallel the speed of occurrence of

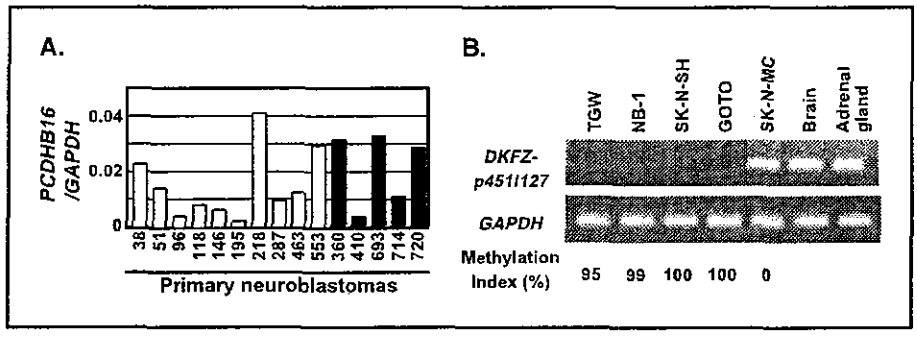

Figure 4. Effects of methylation of the *PCDHB* family and *DKFZp451I127* on gene expression. *A*, *PCDHB16* expression was analyzed by quantitative RT-PCR in 10 primary samples with low methylation (*open columns*) and five primary samples with high methylation (*closed columns*), and no difference was observed between the two groups. *B*, silencing of *DKFZp451I127* by methylation of its promoter CGI. The CGI was methylated in four cell lines, TGW, NB-1, SK-N-SH, and GOTO, whereas it was unmethylated in one cell line, SK-N-MC. *DKFZp451I127* was expressed in SK-N-MC, but not expressed at all in the four cell lines with the promoter methylation.

Table 2. HRs of death by *PCDHB* methylation status in subgroup of known prognostic factors

Stratified by		*PCDHB* methylation	No. cases	No. deaths	HR* (95% CI)	*P*†
Overall		High	67	1	22.1 (5.3-93.4)	< 0.0001
(n = 140)		Low	73	2	1	
N-*myc* amplification	No	High	30	8	12.4 (2.6-58.9)	0.002
(n = 140)		Low	72	2	1	
	Yes	High	37	20	NE	—
		Low	1	0		
TrkA overexpression	Yes	High	20	6	18.3 (2.2-152.6)	0.007
(n = 130)		Low	49	1	1	
	No	High	40	19	NE	
		Low	21	0		
DNA ploidy	Aneuploid	High	17	5	18.3 (2.1-156.7)	0.008
(n = 125)		Low	49	1	1	
	Diploid	High	38	17	NE	
		Low	21	0		
Clinical stages	Stages I, II,	High	8	0	NE	—
(n = 140)	and IVS	Low	52	0		
	Stages III	High	59	28	7.4 (1.8-31.3)	0.006
	and IV	Low	21	2	1	
Age at diagnosis	<1	High	11	3	NE	
(n = 140)	≥1	Low	59	0		
		High	56	25	4.5 (1.1-18.9)	0.043
		Low	14	2	1	

*HR of death for a case with high *PCDHB* methylation compared with a case with low methylation. NE shows not estimable due to no events in at least one category.
†Significance level for a high *PCDHB* methylation to low methylation using Cox proportional model.

methylation. Second, methylation of the *PCDHB* family did not affect gene expression, and there should have been no selection of cells with the *PCDHB* methylation, in contrast to the case of promoter methylation of tumor suppressor genes. Investigation into the mechanism of the intrinsic tendency for methylation of multiple CGIs is necessary. Furthermore, alleviation of the intrinsic tendency could block progression of neuroblastomas and have potential therapeutic value.

Among the six CGI (groups) outside promoter regions analyzed here, CIMP in neuroblastomas preferentially affected four CGI (groups); those of the *PCDHB* family, the *PCDHA* family, *HLP*, and *CYP26C1*. Unexpectedly, three CGIs that are known to be frequently methylated in human colon cancers with CIMP, MINT1, MINT2, and MINT17 (16) were not methylated in neuroblastoma cell lines (data not shown). Among the nine CGIs in promoter regions analyzed, CIMP in neuroblastomas affected only three, those of *RASSF1A*, *BLU*, and *DKFZp451I127*. The nine CGIs were selected based upon previous reports as tumor suppressor genes (*RASSF1A*, *BLU*, *p16*, and *hMLH1*; refs. 21-23), the chromosomal location flanking the *PCDHB* family (*PCDHB1* and *TAF7*), our previous report on the fidelity in inheriting methylation patterns (*p41Arc* and *SIM2*; ref. 19), and the findings here (*DKFZp451I127*). Because gene expression and possibly chromatin structures affect the frequency of *de novo* methylation (24, 25), the available data suggest that CGIs useful to sensitively detect CIMP might vary according to the tumor type.

The influence of CIMP on prognosis was here found to be comparable to that of the currently most reliable marker, N-*myc* amplification, and stronger than *TrkA* overexpression and DNA ploidy on univariate analysis. Subgroup analysis showed that the influence was independent of *TrkA* overexpression, DNA ploidy and age at diagnosis and CIMP had influence even in cases without N-*myc* amplification and in advanced stages. These points strongly indicated CIMP to be a promising new prognostic marker. However, the cutoff values adopted here are tentative, and the HRs obtained could have been overestimated. A validation study using independent samples is necessary for further evaluation. The fact that cases with CIMP contained almost all the cases with N-*myc* amplification suggested that a common molecular mechanism caused both alterations, or that CIMP may lead to N-*myc*

amplification. Whatever the case, the findings might provide clues to molecular mechanisms of neuroblastoma development.

In summary, the present study showed that CIMP is present specifically in neuroblastomas with poor prognosis and that can be sensitively detected by focusing on *PCDHB* methylation. CIMP seems to be a promising new prognostic marker, and its evaluation and investigations into the mechanisms underlying CIMP in neuroblastomas seem warranted.

Acknowledgments

Received 7/27/2004; revised 11/14/2004; accepted 11/24/2004.

Grant support: Grant-in-aid for the Third-term Cancer Control Strategy Program from the Ministry of Health, Labour, and Welfare, Japan and Research Resident Fellowship from the Foundation for Promotion of Cancer Research (M. Abe).

The costs of publication of this article were defrayed in part by the payment of page charges. This article must therefore be hereby marked advertisement in accordance with 18 U.S.C. Section 1734 solely to indicate this fact.

We thank Drs. E. Okochi-Takada and G. S. Goldberg for critical reading of the article and the institutions for participation in the collection of clinical materials.

References

1. Jones PA, Baylin SB. The fundamental role of epigenetic events in cancer. *Nat Rev Genet* 2002;3:415–28.
2. Chen RZ, Pettersson U, Beard C, Jackson-Grusby L, Jaenisch R. DNA hypomethylation leads to elevated mutation rates. Nature 1998;395:89–93.
3. Kondo Y, Kanai Y, Sakamoto M, et al. Genetic instability and aberrant DNA methylation in chronic hepatitis and cirrhosis-A comprehensive *study of loss of heterozygosity and microsatellite* instability at 39 loci and DNA hypermethylation on 8 CpG islands in microdissected specimens from patients with hepatocellular carcinoma. Hepatology 2000;32:970–9.
4. Ushijima T, Morimura K, Hosoya Y, et al. Establishment of methylation-sensitive-representational difference *analysis and isolation of hypo- and hypermethylated* genomic fragments in mouse liver tumors. Proc Natl Acad Sci U S A 1997;94:2284–9.
5. Kaneda A, Takai D, Kaminishi M, Okochi E, Ushijima T. Methylation-sensitive representational difference analysis and its application to cancer research. Ann N Y Acad Sci 2003;983:131–41.
6. *Takai D, Yagi Y, Wakazono K, et al. Silencing of HTR1B* and reduced expression of *EDN1* in human lung cancers, revealed by methylation-sensitive representational difference analysis. Oncogene 2001; 20:7505–13.
7. Kaneda A, Kaminishi M, Yanagihara K, Sugimura T, Ushijima T. Identification of silencing of nine genes in *human gastric cancers. Cancer Res* 2002;62:6645–50.
8. Miyamoto K, Asada K, Fukutomi T, et al. Methylation-associated silencing of heparan sulfate *D-glucosaminyl 3-O-sulfotransferase-2 (3-OST-2)* in human breast, colon, lung and pancreatic cancers. Oncogene 2003;22:274–80.
9. Hagihara A, Miyamoto K, Furuta J, et al. Identification of 27 5′ CpG islands aberrantly methylated and 13 genes silenced in human pancreatic cancers. Oncogene 2004;23:8705–10.
10. Brodeur GM. Neuroblastoma: biological insights into a clinical enigma. Nat Rev. Cancer 2003;3:203–16.
11. Schwab M, Westermann F, Hero B, Berthold F. Neuroblastoma: biology and molecular and chromosomal pathology. Lancet Oncol 2003;4:172–80.
12. Nakagawara A, Arima-Nakagawara M, Scavarda NJ, et al. Association between high levels of expression of the *TRK* gene and favorable outcome in human neuroblastoma. N Engl J Med 1993;328:847–54.
13. Jaenisch R, Bird A. Epigenetic regulation of gene expression: how the genome integrates intrinsic and environmental signals. Nat Genet 2003;33:245–54.
14. Li E. Chromatin modification and epigenetic reprogramming in mammalian development. Nat Rev Genet 2002;3:662–73.
15. Kaneda A, Kaminishi M, Sugimura T, Ushijima T. Decreased expression of the seven ARP2/3 complex genes in human gastric cancers. Cancer Lett 2004; 212:203–10.
16. Toyota M, Ahuja N, Ohe-Toyota M, et al. CpG island methylator phenotype in colorectal cancer. Proc Natl Acad Sci U S A 1999;96:8681–6.
17. Gonzalgo ML, Hayashida T, Bender CM, et al. The role of DNA methylation in expression of the *p19/p16* locus in human bladder cancer cell lines. Cancer Res 1998;58:1245–52.
18. Nguyen C, Liang G, Nguyen TT, et al. Susceptibility of nonpromoter CpG islands to *de novo* methylation in normal and neoplastic cells. J Natl Cancer Inst 2001; 93:1465–72.
19. Ushijima T, Watanabe N, Okochi E, et al. Fidelity of the methylation pattern and its variation in the genome. Genome Res 2003;13:868–74.
20. Yamashita K, Dai T, Dai Y, Yamamoto F, Perucho M. Genetics supersedes epigenetics in colon cancer phenotype. Cancer Cell 2003;4:121–31.
21. Agathanggelou A, Dallol A, Zochbauer-Muller S, et al. Epigenetic inactivation of the candidate 3p21.3 suppressor gene *BLU* in human cancers. Oncogene 2003; 22:1580–8.
22. Takita J, Hayashi Y, Nakajima T, et al. The *p16 (CDKN2A)* gene is involved in the growth of neuroblastoma cells and its expression is associated with prognosis of neuroblastoma patients. Oncogene 1998; 17:3137–43.
23. Harada K, Toyooka S, Maitra A, et al. Aberrant promoter methylation and silencing of the *RASSF1A* gene in pediatric tumors and cell lines. Oncogene 2002; 21:4345–9.
24. De Smet C, Loriot A, Boon T. Promoter-dependent mechanism leading to selective hypomethylation within the 5′ region of gene *MAGE-A1* in tumor cells. Mol Cell Biol 2004;24:4781–90.
25. Richards EJ, Elgin SC. Epigenetic codes for heterochromatin formation and silencing: rounding up the usual suspects. Cell 2002;108:489–500.

Oncogene (2005) 24, 938–944

www.nature.com/onc

Protein stability and function of p73 are modulated by a physical interaction with RanBPM in mammalian cultured cells

Sonja Kramer[1], Toshinori Ozaki[1], Kou Miyazaki[1], Chiaki Kato[1], Takayuki Hanamoto[1] and Akira Nakagawara*,[1]

[1]*Division of Biochemistry, Chiba Cancer Center Research Institute, 666-2 Nitona, Chuoh-ku, Chiba 260-8717, Japan*

Upon a certain DNA damage including cisplatin treatment, p73 is stabilized and exerts its growth-suppressive and/or proapoptotic function. However, the precise molecular basis by which the intracellular levels of p73 are regulated remains unclear. In the present study, we have identified RanBPM as a novel binding partner of p73α by yeast-based two-hybrid screening, and also found that RanBPM has an ability to stabilize p73α. GST pull-down assays and co-immunoprecipitation experiments revealed that RanBPM directly bound to the extreme COOH-terminal region of p73α, whereas it failed to interact with p53. Co-expression of RanBPM with p73α resulted in the nuclear translocation of RanBPM, and both proteins co-localized in cell nucleus as examined by indirect immunofluorescent staining. It is worth noting that the expression of RanBPM inhibited the ubiquitination of p73α, and thereby prolonged its half-life. Subsequent studies demonstrated that the proapoptotic activity of p73α was significantly enhanced in the presence of RanBPM. Taken together, our present findings implicate a novel role for RanBPM in the regulation of p73 stability and function.
Oncogene (2005) **24,** 938–944. doi:10.1038/sj.onc.1208257
Published online 22 November 2004

Keywords: p53; p73; RanBPM; two-hybrid; ubiquitination

p73 is a newly identified p53-related nuclear transcription factor, and functions to promote cell cycle arrest and/or apoptosis (Kaghad *et al.*, 1997). These cellular roles of p73 are largely attributed to its ability to transactivate specific target genes. In contrast to p53, p73 is expressed as multiple isoforms arising from either alternative splicing or alternative promoter usage (Melino *et al.*, 2002). Although functional differences among the splicing isoforms with different COOH-termini remain unclear, NH_2-terminally truncated forms of p73 (ΔNp73) have an oncogenic potential and exhibit a dominant-negative behavior toward wild-type p73 as well as p53 (Pozniak *et al.*, 2000; Nakagawa *et al.*, 2002; Stiewe *et al.*, 2002).

Steady-state levels of p73 are kept extremely low under normal conditions, however, p73 is significantly induced at protein level in response to a certain genotoxic stress including cisplatin treatment, which is mediated by a nuclear nonreceptor tyrosine kinase c-Abl (Agami *et al.*, 1999; Gong *et al.*, 1999; Yuan *et al.*, 1999). c-Abl binds to the PXXP motif of p73 and phosphorylates p73 at Tyr-99. Alternatively, Ren *et al.* (2002) reported that protein kinase Cδ catalytic fragment phosphorylates p73 at Ser-289, and increases its stability, suggesting that post-translational modification such as phosphorylation might contribute to increase the stability of p73. Protein phosphorylation has been shown to be involved in the initiation of protein ubiquitination by E3 ubiquitin ligase (Carrano *et al.*, 1999; Ganoth *et al.*, 2001). As described previously (Balint *et al.*, 1999; Lee and La Thangue, 1999), p73 is regulated at least in part by the protein degradation process through the ubiquitin–proteasome system. Additionally, Lee and La Thangue (1999) described that the COOH-terminal region of p73α might have a regulatory role in the proteasome-dependent degradation of p73. Recently, we have found that MM1 and RACK1 interact with the extreme COOH-terminal region of p73α, and regulate its transcriptional activity as well as proapoptotic function (Watanabe *et al.*, 2002; Ozaki *et al.*, 2003). However, these interactions did not have a detectable effect on the intracellular levels of p73α.

To identify the possible cellular protein(s) involved in the regulation of p73 protein stability, we screened a cDNA library derived from human fetal brain using the extreme COOH-terminal region of p73α (amino-acid residues 551–636) as a bait in a yeast-based two-hybrid system. After screening of approximately 5×10^5 transformants, 12 independent clones exhibited a high level of β-galactosidase activity, and subsequent sequence analysis revealed that three out of them encoded the overlapping regions of RanBPM (Figure 1a). RanBPM was initially identified as a cellular protein that can interact with Ran nuclear–cytoplasmic transport protein (Nakamura *et al.*, 1998; Nishitani *et al.*, 2001), and contained the putative SPRY domain which might be involved in protein–protein interactions (Ponting *et al.*, 1997). Although most of the Ran-binding proteins play an important role in nucleocytoplasmic transport, it is

*Correspondence: A Nakagawara;
E-mail: akiranak@chiba-ccri.chuo.chiba.jp
Received 16 July 2004; revised 4 October 2004; accepted 6 October 2004; published online 22 November 2004

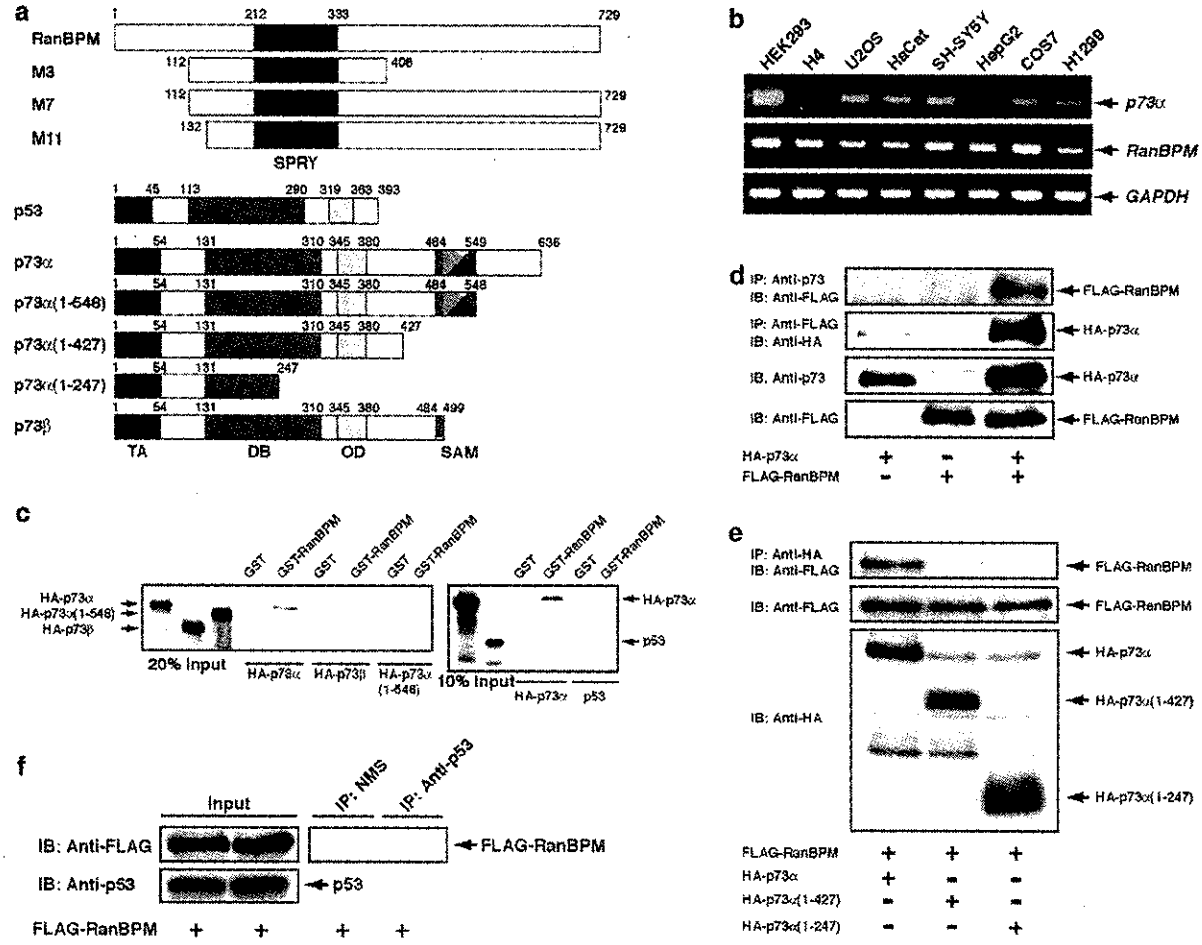

Figure 1 Identification of RanBPM as a binding partner of p73. (**a**) The three overlapping RanBPM clones (M3, M7 and M11) isolated from the yeast two-hybrid screening along with the full-length RanBPM are shown. The putative SPRY domain (amino-acid residues 212–333) is indicated. Structures of p73 and p53 are also shown. TA, transactivation domain; DB, DNA-binding domain; OD, oligomerization domain; SAM, sterile α motif domain. Amino-acid numbering was relative to first methionine, which represents position +1. (**b**) Expression of *RanBPM* and *p73*. Total RNA prepared from the indicated cell lines were incubated with SuperScript II reverse transcriptase (Invitrogen, Carlsbad, CA, USA), and generated cDNAs were amplified by PCR in the presence of primers specific for *p73* (top panel), *RanBPM* (middle panel) or *GAPDH* (bottom panel). (**c**) GST pull-down assay. *In vitro* translated ^{35}S-labeled p73α, p73β, p73α (1–548) or p53 was incubated with bacterially expressed GST or GST-RanBPM(112–408) for 2 h at 4°C. Bound complexes were recovered on the glutathione–sepharose beads (Amersham Pharmacia Biotech, Piscataway, NJ, USA), washed extensively with the binding buffer (50 mM Tris–HCl, pH 7.5, 150 mM NaCl, 0.1% Nonidet P-40, 1 mM EDTA, and 1 mM phenylmethylsulfonyl fluoride), and then boiled in SDS sample buffer. Bound proteins were resolved by 10% SDS–polyacrylamide gel, and analysed by autoradiography. The input of the radio-labeled proteins used in the binding reaction is also shown. (**d**) p73α interacts with RanBPM in mammalian cultured cells. COS7 cells transfected with the indicated expression plasmids were lysed in 25 mM Tris–HCl, pH 8.0, 137 mM NaCl, 1% Triton X-100 and 1 mM phenylmethylsulfonyl fluoride. Whole-cell lysates were immunoprecipitated with anti-p73 antibody (Ab-4, NeoMarkers, Fremont, CA, USA) or anti-FLAG (M2, Sigma, St Louis, MO, USA), and subjected to immunoblotting with anti-FLAG (first panel) or with anti-HA (12CA5, Roche Molecular Biochemicals, Indianapolis, IN, USA) antibody (second panel), respectively. Separate aliquots of the lysates were immunoblotted with anti-p73 (third panel) or anti-FLAG antibody (fourth panel) to confirm the expression of FLAG-RanBPM or HA-p73α, respectively. (**e**) COOH-terminal region of p73α is required for the interaction with RanBPM. COS7 cells were co-transfected with the indicated combinations of the expression plasmids, and whole-cell lysates were immunoprecipitated with anti-HA antibody, followed by immunoblotting with anti-FLAG antibody (top panel). Cell lysates were immunoblotted as a control for FLAG-RanBPM (middle panel), HA-p73α and HA-p73α derivatives (bottom panel) in the input lysate. (**f**) p53 does not bind to RanBPM. Cell lysates prepared from COS7 cells transfected with FLAG-RanBPM were immunoprecipitated with the normal mouse serum (NMS, Jackson ImmunoResearch Laboratories, West Grove, PA, USA) or anti-p53 antibodies (DO-1 plus PAb1801, Oncogene Research Products, Cambridge, MA, USA). Immunoprecipitates were analysed by immunoblotting with anti-FLAG antibody (right panel). Left panels show the Western blotting with anti-FLAG, or anti-p53 antibody to monitor the expression level of FLAG-RanBPM or the endogenous p53, respectively

unlikely that RanBPM is involved in this process (Nishitani *et al*., 2001). Alternatively, Nakamura *et al*. (1998) reported that RanBPM might be involved in reorganization of the microtubule network; however, the precise function of RanBPM remains unknown.

Consistent with the previous observations (Rao *et al*., 2002), *RanBPM* was expressed in various cell lines (Figure 1b). To confirm the interaction between RanBPM and p73, we performed GST pull-down assays using a GST fusion protein containing RanBPM

(112–408) and *in vitro* translated ^{35}S-labeled p73α, p73β, p73α(1–548) or p53. GST alone was employed as a negative control. As shown in Figure 1c, radio-labeled p73α was pulled down by GST-RanBPM(112–408) but not by GST alone. However, p73β and p73α(1–548), which lack the extreme COOH-terminal portion of p73α, were no longer able to interact with GST-RanBPM(112–408). In addition, p53 failed to bind to GST-RanBPM(112–408). In good agreement with the yeast two-hybrid results, these observations suggest that the extreme COOH-terminal portion of p73α is responsible for the physical interaction with RanBPM. Next, we performed co-immunoprecipitation experiments to confirm their interaction in cells. To this end, cell lysates prepared from COS7 cells co-transfected with HA-tagged p73α and FLAG-tagged full-length RanBPM were immunoprecipitated with anti-p73 or anti-FLAG antibody, followed by immunoblotting with anti-FLAG or anti-HA antibody, respectively. As shown in Figure 1d, HA-p73α co-immunoprecipitated with FLAG-RanBPM. Under our experimental conditions, HA-p73α(1–427) and HA-p73α(1–247) did not co-immunoprecipitate with FLAG-RanBPM (Figure 1e). In contrast to full-length p73α, the anti-p53 immunoprecipitates did not contain FLAG-RanBPM (Figure 1f). Taken together, our results suggest that RanBPM has an ability to interact with p73α but not with p53 in mammalian cultured cells.

Previous immunostaining studies have shown that p73α is exclusively localized in cell nucleus (Jost *et al.*, 1997), while RanBPM could distribute to the cell nucleus, perinuclear region and cytoplasm (Nishitani *et al.*, 2001; Umeda *et al.*, 2003). To examine the subcellular localization of RanBPM in the presence or absence of p73α, COS7 cells were transfected with the indicated expression plasmids, and the indirect immunofluorescent staining was performed. As shown in Figure 2a and b, FLAG-RanBPM and HA-p73α were detected largely in the cytoplasm and cell nucleus, respectively. Of note, when FALG-RanBPM was co-expressed with HA-p73α, a fraction of FLAG-RanBPM translocated into cell nucleus, and co-localized with nuclear HA-p73α (Figure 2c–e). To confirm this issue, transfected COS7 cells were fractionated into nuclear and cytoplasmic fractions, and their subcellular localizations were analysed by immunoblotting. The purity of the nuclear and cytoplasmic fractions was examined by immunoblotting with anti-Lamin B and anti-α-tubulin antibody, respectively. Consistent with the indirect immunofluorescent staining, co-expression of FLAG-RanBPM with HA-p73α resulted in a significant nuclear accumulation of FLAG-RanBPM, whereas FLAG-RanBPM alone was detected in the cytoplasmic fraction (Figure 2f). In addition, the amounts of nuclear HA-p73α seemed to be increased in the presence of FLAG-RanBPM. It is thus likely that RanBPM interacts with p73α in cell nucleus, and could affect the stability of p73α.

To test whether RanBPM could affect the stability of p73α, COS7 cells were co-transfected with the constant amount of HA-p73α together with or without the

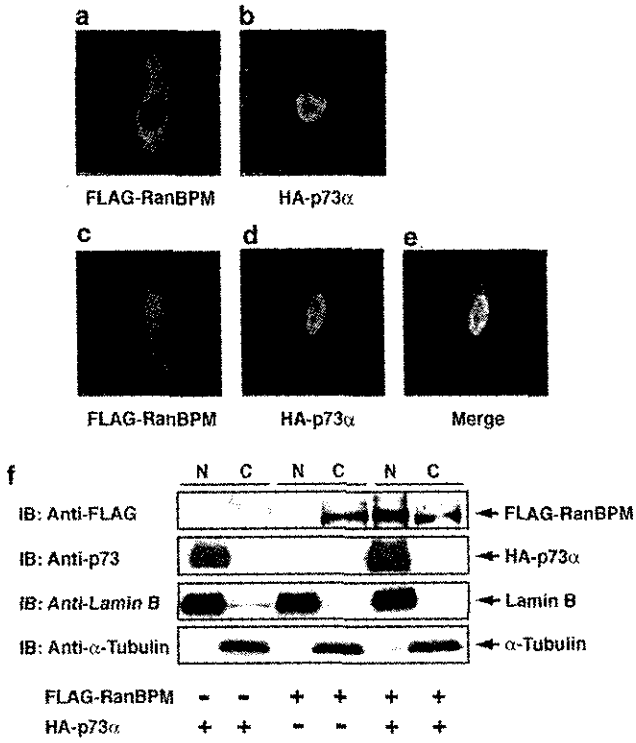

Figure 2 Subcellular distribution of RanBPM in the presence of p73. (a–e) Nuclear co-localization of p73α and RanBPM by immunofluorescence. COS7 cells were transfected with FLAG-RanBPM (a), HA-p73α (b) or FLAG-RanBPM and HA-p73α (c–e). At 48 h after transfection, cells were fixed in 20% methanol and incubated with anti-FLAG (red) and anti-HA antibody (green) (Medical and Biological Laboratories, Nagoya, Japan), followed by the incubation with the rhodamine- and FITC-conjugated secondary antibodies (Jackson ImmunoResearch Laboratories), respectively. Cells were then examined under a confocal scanning laser microscope. The merged images of the two signals are displayed in yellow (e). (f) Fractionation of COS7 cell extracts. COS7 cells were transfected with the indicated expression plasmids. At 48 h after transfection, cells were fractionated into nuclear (N) and cytoplasmic (C) fractions, and then analysed directly by immunoblotting with anti-FLAG (first panel) or anti-p73 antibody (second panel). The nuclear or cytoplasmic fraction was confirmed by immunoblotting with anti-Lamin B (Ab-1, Oncogene Research Products) (third panel) or anti-α-tubulin antibody (DM1A, Cell Signaling Technology, Beverly, MA, USA) (fourth panel), respectively

increasing amounts of FLAG-RanBPM. As shown in Figure 3a, the amount of HA-p73α was markedly increased in the presence of FLAG-RanBPM in a dose-dependent manner, whereas the expression level of p73α mRNA remained unchanged. On the other hand, FLAG-RanBPM had no significant effect on the levels of exogenous p53 (Figure 3b). Similar results were also obtained in p53-deficient H1299 cells (data not shown). We next sought to determine the half-life of p73α in the presence of RanBPM. For this purpose, COS7 cells were transfected with HA-p73α together with or without FLAG-RanBPM. At 24 h after transfection, cells were treated with cycloheximide. At the indicated time periods, cell lysates were analysed for HA-p73α by immunoblotting. In accordance with the previous reports (Lee and La Thangue, 1999; Ohtsuka *et al.*,

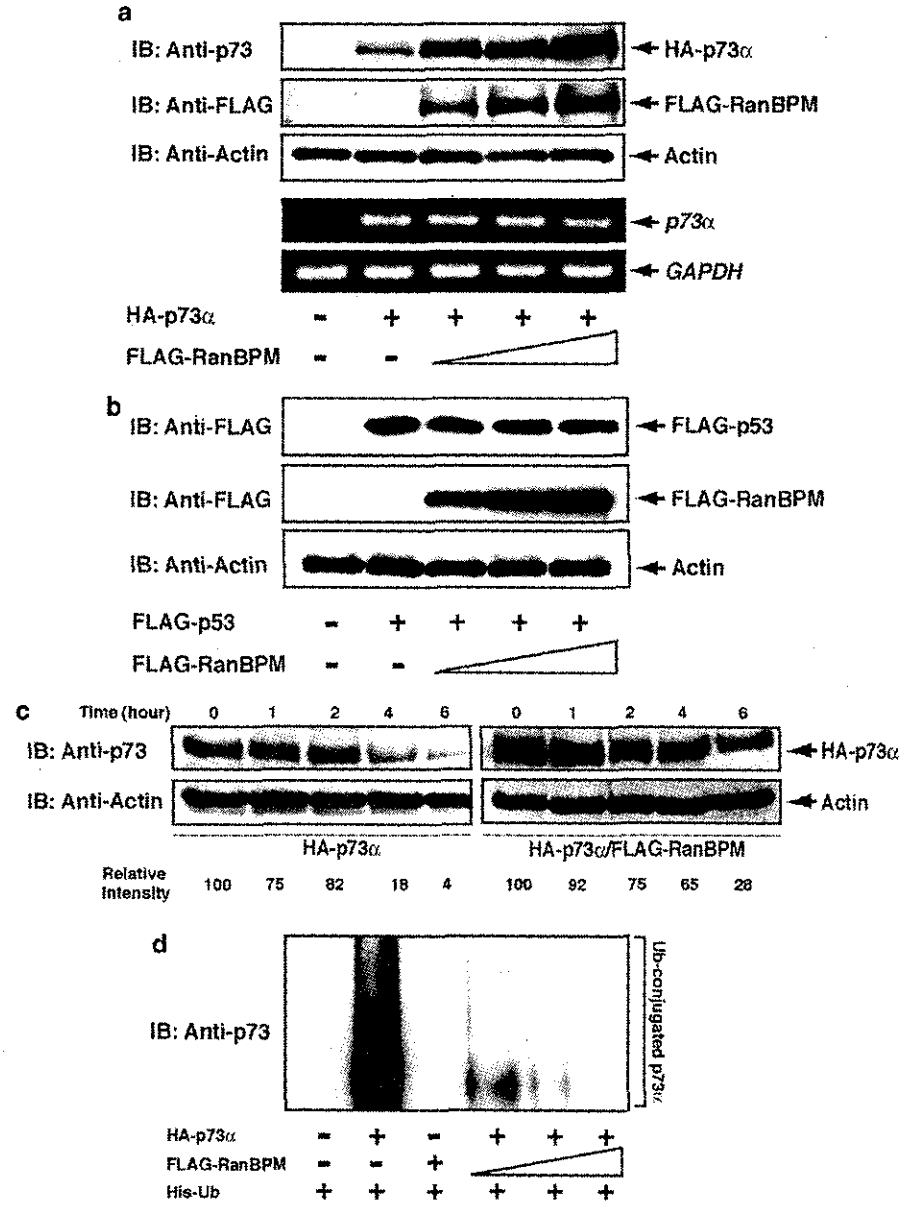

Figure 3 RanBPM increases the stability of p73 but not of p53. (**a**) RanBPM increases the amounts of p73α. COS7 cells were co-transfected with the constant amount of HA-p73α (0.5 μg) together with or without the increasing amounts of FLAG-RanBPM (0.5, 1.0 and 1.5 μg). The total amount of plasmid DNA was kept constant (2 μg) with pcDNA3. At 48 h after transfection, cell lysates or total RNA were prepared, and subjected to immunoblotting with the indicated antibodies (upper panels) or RT–PCR analysis (lower panels). Immunoblotting for actin (20–33, Sigma Chemical Co.) serves as a loading control. (**b**) RanBPM does not affect the amounts of p53. COS7 cells were co-transfected with the indicated combinations of the expression plasmids, and were processed for immunoblotting as described above. (**c**) RanBPM increases the half-life of p73α. COS7 cells were transfected with HA-p73α alone (0.5 μg) (left panels) or together with FLAG-RanBPM (1.5 μg) (right panels). At 24 h post-transfection, cells were treated with cycloheximide (100 μg/ml) and harvested at the indicated time periods. Cell lysates were used for immunoblotting with the indicated antibodies. The intensity of the bands was quantified by using densitometry. (**d**) RanBPM inhibits the ubiquitination of p73α. COS7 cells were co-transfected with the constant amount of HA-p73α (0.5 μg) and His-tagged ubiquitin (Ub) (0.5 μg), together with or without the increasing amounts of FLAG-RanBPM (0.5, 1.0 and 1.5 μg). At 24 h post-transfection, cells were treated with 20 μM MG-132 for 6 h before being harvested. His-tagged ubiquitin-containing protein complexes were pulled down with Ni^{2+}-agarose beads (QIAGEN, Valencia, CA, USA), and subsequently resolved by 10% SDS–polyacrylamide gel electrophoresis, followed by immunoblotting with anti-p73 antibody

2003), ectopically expressed p73α had a half-life of less than 4 h, whereas the degradation rate of HA-p73α was slower in FLAG-RanBPM-expressing cells (Figure 3c). Thus, it is likely that the RanBPM-dependent stabilization of p73α is attributed to the clear increase in the half-life of p73α.

As described (Balint *et al*., 1999), the stability of p73 is regulated at least in part through the ubiquitin–proteasome pathway. These observations prompted us to determine whether RanBPM could prevent the ubiquitination of p73. COS7 cells were transfected with HA-p73α- and His-tagged ubiquitin, or in combination

with the increasing amounts of FLAG-RanBPM. At 24 h after transfection, cells were treated with MG-132 for 6 h. His-ubiquitinated proteins were purified by Ni^{2+}-agarose beads, and then analysed by immunoblotting with the anti-p73 antibody. As shown in Figure 3d, the slower migrating ubiquitinated forms of p73α were detectable in the absence of FLAG-RanBPM. Intriguingly, the ubiquitination levels of p73α were significantly reduced in cells expressing FLAG-RanBPM, suggesting that RanBPM stabilizes p73α by inhibiting its ubiquitination.

To determine whether RanBPM could affect the transcriptional activity of p73α, H1299 cells were transiently transfected with a constant amount of the expression plasmid for HA-p73α, together with the p53/p73-responsive $p21^{WAF1}$ or *MDM2* luciferase reporter constructs in the presence or absence of increasing amounts of the FLAG-RanBPM expression plasmid. As shown in Figure 4a, expression of FLAG-RanBPM enhanced the ability of p73α to transactivate the $p21^{WAF1}$ and *MDM2* promoters in a dose-dependent manner. To extend the functional significance of their interaction, we examined the possible effect of RanBPM on the p73α-mediated apoptosis. H1299 cells were transfected with HA-p73α, FLAG-RanBPM, or HA-p73α and FLAG-RanBPM. The β-galactosidase was used as a marker to visualize the transfected cells. At 48 h post transfection, the number of β-galactosidase-positive cells was scored. As shown in Figure 4b, the number of β-galactosidase-positive cells expressing FLAG-RanBPM was similar to that detected in the empty plasmid-transfected cells. Consistent with the previous report (Watanabe *et al.*, 2002), expression of HA-p73α resulted in a clear decrease in the number of β-galactosidase-positive cells. Of note, co-expression of HA-p73α with FLAG-RanBPM significantly reduced the number of β-galactosidase-positive cells as compared with that observed in cells expressing HA-p73α alone. In addition, we performed a colony formation assay. H1299 cells were transfected with HA-p73α, FLAG-RanBPM or HA-p73α plus FLAG-RanBPM, and the transfected cells were selected in the presence of G418. After 2 weeks of selection, drug-resistant colonies were fixed and stained with Giemsa's solution. In accordance with the β-galactosidase assay, FLAG-RanBPM expression did not affect the colony formation as compared with the empty plasmid-transfected control, whereas co-expression of HA-p73α with FLAG-RanBPM reduced the colony formation even more efficiently than HA-p73α alone (Figure 4c). Considering that p73α efficiently induced apoptosis in H1299 cells (Di Como *et al.*, 1999; Zeng *et al.*, 1999), these results suggest that RanBPM increases the proapoptotic activity of p73α. To further confirm this issue, H1299 cells were transiently transfected with a constant amount of the GFP expression plasmid along with the indicated combinations of the expression plasmids. At 48 h after transfection, transfected cells were identified by fluorescence microscopy for the appearance of green fluorescence, and the number of GFP-positive cells with condensed and fragmented nuclei was counted. As shown in Figure 4d, co-expression of HA-p73α with FLAG-RanBPM increased the number of apoptotic cells as compared with that resulting from expression of HA-p73α alone. Taken together, our present results strongly suggest that RanBPM-mediated stabilization of p73α is critical for its effects on transcriptional activation as well as apoptosis.

Recently, it has been shown that a variety of cellular proteins could interact with RanBPM, including MET, androgen receptor, HIPK2, USP11, Twa1, calbindin D28K and $p75^{NTR}$, suggesting that RanBPM is involved in diverse biological processes (Ideguchi *et al.*, 2002; Rao *et al.*, 2002; Wang D *et al.*, 2002; Wang Y *et al.*, 2002; Bai *et al.*, 2003; Lutz *et al.*, 2003; Umeda *et al.*, 2003). In the present study, we demonstrated that RanBPM increased the stability of p73α by reducing its ubiquitination levels. An important question raised by our results is how RanBPM stabilize p73α. Intriguingly, Ideguchi *et al.* (2002) described that RanBPM is associated with the deubiquitination enzyme USP11, which belongs to the ubiquitin hydrolase family. Considering that p53 is stabilized by direct deubiquitination by the deubiquitination enzyme HAUSP (Li *et al.*, 2002), it is likely that RanBPM could bind to USP11 and promote deubiquitination of p73α by recruiting USP11 to p73α; however, further studies will be required to determine this issue.

Alternatively, Lee and La Thangue (1999) found that p73β is much more stable than p73α, suggesting that the unique COOH-terminal portion of p73α might be critical for degradation by the ubiquitin–proteasome system. According to our present results, RanBPM bound to p73α through its extreme COOH-terminal region, whereas it failed to interact with p73β. Thus, it is plausible that RanBPM might increase the steady-state levels of p73α by masking p73α COOH-terminal lysine residues, which could be the sites for ubiquitin ligation, and/or disrupting the interaction of p73α with unknown proteins required for ubiquitination-mediated proteolysis. These possibilities are currently under investigation. Elucidation of the detailed molecular mechanism underlying the RanBPM-dependent stabilization of p73α would be necessary for better understanding of p73 turnover.

Another finding of the present study is that, under our experimental conditions, cytoplasmic RanBPM became nuclear in the presence of p73α overexpression. Given that RanBPM is localized in both the cytoplasm and nucleus (Nakamura *et al.*, 1998; Nishitani *et al.*, 2001), it is probable that p73α might have an ability to promote nuclear translocation of RanBPM through the physical interaction between them. As described previously, wild-type p53 is predominantly localized in the cytoplasm of many neuroblastoma cells (Moll *et al.*, 1996). The abnormal cytoplasmic distribution of p53 might be attributed at least in part to the interaction with Parc, which acts as a cytoplasmic anchor protein for p53 (Nikolaev *et al.*, 2003). Interestingly, Goldschneider *et al.* (2004) found that enforced expression of p73α in neuroblastoma-derived SH-SY5Y cells significantly enhances the nuclear accumulation of wild-type p53 and

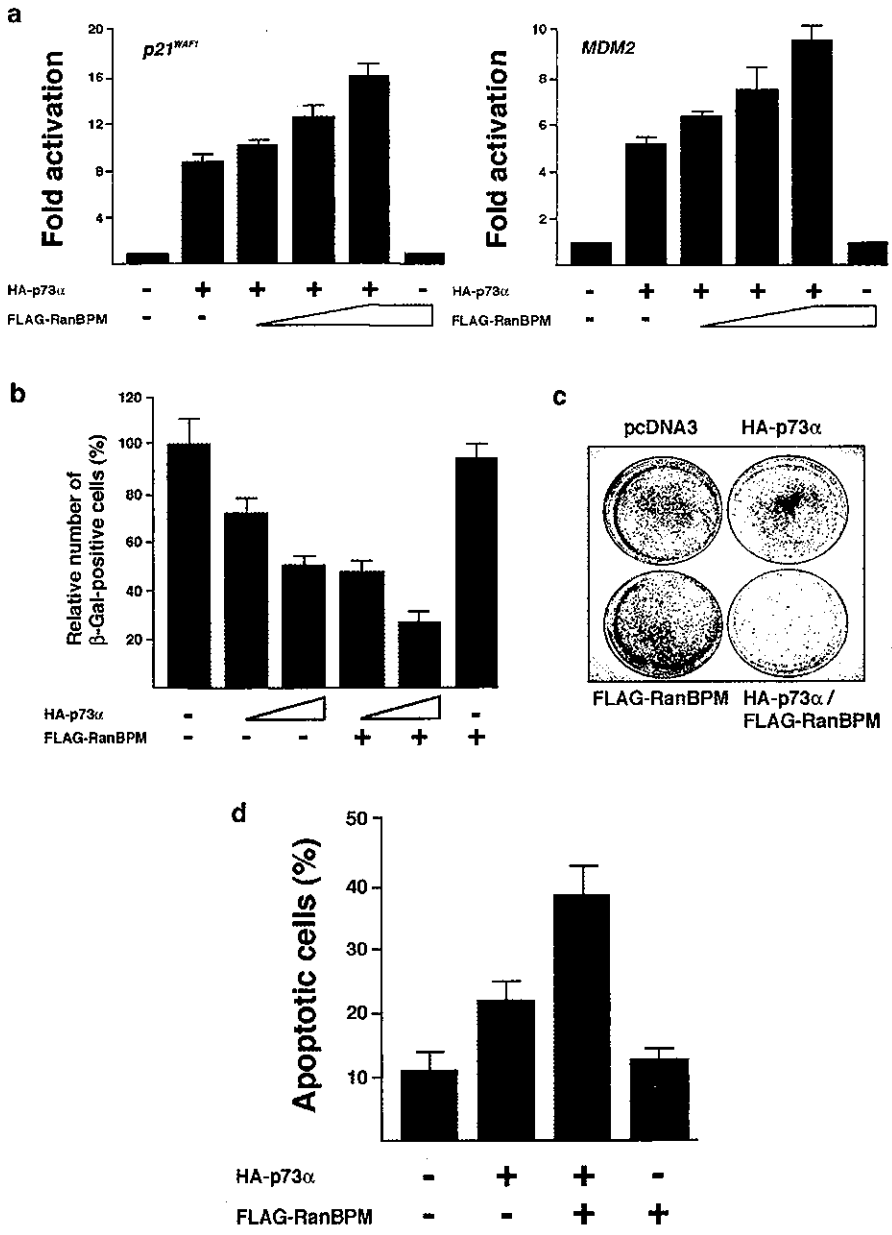

Figure 4 RanBPM enhances p73 function. (**a**) RanBPM enhances the transcriptional activity of p73α. p53-deficient H1299 cells were co-transfected with 25 ng of the expression plasmid for HA-p73α together with 100 ng of p53/p73-responsive *p21*^{WAF1} (left panel) or *MDM2* (right panel) luciferase reporter construct, and 10 ng of the *Renilla* luciferase plasmid (pRL-TK, Promega Corp., Madison, WI, USA), in the presence or absence of increasing amounts of the FLAG-RanBPM expression plasmid (25, 50, or 100 ng). At 48 h after transfection, cells were lysed and their luciferase activities were measured. Firefly luminescence signal was normalized based on the *Renilla* luminescence signal. (**b**) RanBPM stimulates the p73α-mediated growth suppression. H1299 cells were co-transfected with the indicated combinations of the expression plasmid together with the constant amount of the expression plasmid for β-galactosidase (125 ng) (pCH110, Amersham Pharmacia Biotech). At 48 h after transfection, transfected cells were identified by staining with 5-bromo-4-chloro-3-indolyl-β-D-galactopyranoside (X-gal). The relative percentage of β-gal-positive cells represents the ratio of the number of β-gal-positive cells to that of those transfected with pcDNA3 alone. (**c**) Colony formation assay. H1299 cells were transfected with HA-p73α (200 ng), FLAG-RanBPM (750 ng) or HA-p73α (200 ng) plus FLAG-RanBPM (750 ng). Total amount of plasmid DNA was kept constant (1 μg) with pcDNA3, and pcDNA3 alone was used as a negative control. At 2 days after transfection, cells were selected with G418 (400 μg/ml) for 2 weeks. G418-resistant colonies were fixed in methanol, and stained with Giemsa's solution. Representative dishes of three independent experiments are shown. (**d**) RanBPM enhances the p73α-mediated apoptosis. H1299 cells transfected with 0.2 μg of the GFP expression plasmid and 0.5 μg of the HA-p73α expression plasmid together with or without 1.5 μg of the FLAG-RanBPM expression plasmid. At 48 h after transfection, transfected cells were identified by the presence of green fluorescence. Cell nucleus was stained with DAPI to reveal nuclear condensation and fragmentation. The number of GFP-positive cells with apoptotic nuclei was scored

restores its function, indicating that p73α displaces p53 from the cytoplasmic complex containing Parc. It is thus likely that p73α could modulate cellular proteins/pathways that specifically regulate nuclear import and export of RanBPM. Since RanBPM is associated with a variety of nuclear proteins, p73α might play a critical role in regulating nuclear function of RanBPM.

Acknowledgements
We are grateful to Dr S Sakiyama for helpful discussion. This work was supported in part by a Grant-in-Aid from the Ministry of Health and Welfare for a New 10-Year Strategy for Cancer Control, a Grant-in-Aid for Scientific Research on Priority Areas, a Grant-in-Aid for Scientific Research (B) from the Ministry of Education, Science, Sports and Culture, Japan, and a found from the Hisamitsu Pharmaceutical Company.

References

Agami R, Blandino G, Oren M and Shaul Y. (1999). *Nature*, **399**, 809–813.
Bai D, Chen H and Huang BR. (2003). *Biochem. Biophys. Res. Commun.*, **309**, 552–557.
Balint E, Bates S and Vousden KH. (1999). *Oncogene*, **18**, 3923–3929.
Carrano AC, Eytan E, Hershko A and Pagano M. (1999). *Nat. Cell Biol.*, **1**, 193–199.
Di Como CJ, Gaiddon C and Prives C. (1999). *Mol. Cell. Biol.*, **19**, 1438–1449.
Ganoth D, Bornstein G, Ko TK, Larsen B, Tyers M, Pagano M and Hershko A. (2001). *Nat. Cell Biol.*, **3**, 321–324.
Goldschneider D, Blanc E, Raguenez G, Barrois M, Legrand A, Le Roux G, Haddada H, Bebard J and Douc-Rasy S. (2004). *J. Cell Sci.*, **117**, 293–301.
Gong J, Costanzo A, Yang H-Q, Melino G, Kaelin WG, Levrero M and Wang JYJ. (1999). *Nature*, **399**, 806–809.
Ideguchi H, Ueda A, Tanaka M, Yang J, Tsuji T, Ohno S, Hagiwara E, Aoki A and Ishigatsubo Y. (2002). *Biochem. J.*, **367**, 87–95.
Jost C, Marin M and Kaelin WG. (1997). *Nature*, **389**, 191–194.
Kaghad M, Bonnet H, Yang A, Creancier L, Biscan JC, Valent A, Minty A, Chalon P, Lelias JM, Dumont X, Ferrara P, McKeon F and Caput D. (1997). *Cell*, **90**, 809–819.
Lee C-W and La Thangue NB. (1999). *Oncogene*, **18**, 4171–4181.
Li M, Chen D, Shiloh A, Luo J, Nikolaev AY, Qin J and Gu W. (2002). *Nature*, **416**, 648–653.
Lutz W, Frank EM, Craig TA, Thompson R, Venters RA, Kojetin D, Cavanagh J and Kumar R. (2003). *Biochem. Biophys. Res. Commun.*, **303**, 1186–1192.
Melino G, De Laurenzi V and Vousden KH. (2002). *Nat. Rev. Cancer*, **2**, 605–615.
Moll UM, Ostermeyer AG, Haladay R, Winkfield B, Frazier M and Zambetti G. (1996). *Mol. Cell. Biol.*, **16**, 1126–1137.
Nakagawa T, Takahashi M, Ozaki T, Watanabe K, Todo S, Mizuguchi H, Hayakawa T and Nakagawara A. (2002). *Mol. Cell. Biol.*, **22**, 2575–2585.
Nakamura M, Masuda H, Horii J, Kuma K, Yokoyama N, Ohba T, Nishitani H, Miyata T, Tanaka M and Nishimoto T. (1998). *J. Cell Biol.*, **143**, 1041–1052.
Nikolaev AY, Li M, Puskas N, Qin J and Gu W. (2003). *Cell*, **112**, 29–40.
Nishitani H, Hirose E, Uchimura Y, Nakamura N, Umeda M, Nishii K, Mori N and Nishimoto T. (2001). *Gene*, **272**, 25–33.
Ohtsuka T, Ryu H, Minamishima YA, Ryo A and Lee SW. (2003). *Oncogene*, **22**, 1678–1687.
Ozaki T, Watanabe K, Nakagawa T, Miyazaki K, Takahashi M and Nakagawara A. (2003). *Oncogene*, **22**, 3231–3242.
Ponting C, Schultz J and Bork P. (1997). *Trends Biochem. Sci.*, **22**, 193–194.
Pozniak CD, Radinovic S, Yang A, McKeon F, Kaplan DR and Miller FD. (2000). *Science*, **289**, 304–306.
Rao MA, Cheng H, Quayle AN, Nishitani H, Nelson CC and Rennie PS. (2002). *J. Biol. Chem.*, **277**, 48020–48027.
Ren J, Datta R, Shioya H, Li Y, Oki E, Biedermann V, Bharti A and Kufe D. (2002). *J. Biol. Chem.*, **277**, 33758–33765.
Stiewe T, Zimmermann S, Frilling A, Esche H and Putzer BM. (2002). *Cancer Res.*, **62**, 3598–3602.
Umeda M, Nishitani H and Nishimoto T. (2003). *Gene*, **303**, 47–54.
Wang D, Li Z, Messing EM and Wu G. (2002). *J. Biol. Chem.*, **277**, 36216–36222.
Wang Y, Schneider M, Li X, Duttenhofer I, Debatin K-M and Hug H. (2002). *Biochem. Biophys. Res. Commun.*, **297**, 148–153.
Watanabe K, Ozaki T, Nakagawa T, Miyazaki K, Takahashi M, Hosoda M, Hayashi S, Todo S and Nakagawara A. (2002). *J. Biol. Chem.*, **277**, 15113–15123.
Yuan Z-M, Shioya H, Ishiko T, Sun X, Gu J, Huang YY, Lu H, Kharbanda S, Weichselbaum R and Kufe D. (1999). *Nature*, **399**, 814–817.
Zeng X, Chen L, Jost CA, Maya R, Keller D, Wang X, Kaelin WG, Oren M, Chen J and Lu H. (1999). *Mol. Cell. Biol.*, **19**, 3257–3266.

Int. J. Cancer: **112**, 365–375 (2004)

Publication of the International Union Against Cancer

LOW EXPRESSION OF HUMAN TUBULIN TYROSINE LIGASE AND SUPPRESSED TUBULIN TYROSINATION/DETYROSINATION CYCLE ARE ASSOCIATED WITH IMPAIRED NEURONAL DIFFERENTIATION IN NEUROBLASTOMAS WITH POOR PROGNOSIS

Chiaki KATO[1,2], Kou MIYAZAKI[1], Atsuko NAKAGAWA[3], Miki OHIRA[1], Yohko NAKAMURA[1], Toshinori OZAKI[1], Toshio IMAI[2] and Akira NAKAGAWARA[1]*

[1]*Division of Biochemistry, Chiba Cancer Center Research Institute, Chiba, Japan*
[2]*Department of Physiologic Chemistry Faculty of Science, Toho University, Chiba, Japan*
[3]*Second Department of Pathology, Aichi Medical University, Nagakute, Japan*

Neuroblastoma (NBL), one of the most common childhood solid tumors, has a distinct nature in different prognostic subgroups. However, the precise mechanism underlying this phenomenon remains largely unknown. To understand the molecular and genetic bases of neuroblastoma, we have generated its cDNA libraries and identified a human ortholog of *tubulin tyrosine ligase* gene (*hTTL/Nbla0660*) as a differentially expressed gene at high levels in a favorable subset of the tumor. Tubulin is subjected to several types of evolutionarily conserved posttranslational modification, including tyrosination and detyrosination. Tubulin tyrosine ligase catalyzes ligation of the tyrosine residue to the COOH terminus of the detyrosinated form of α-tubulin. The measurement of *hTTL* mRNA expression in 74 primary neuroblastomas by quantitative real-time reverse transcription-PCR revealed that its high expression was significantly associated with favorable stages (1, 2 and 4s; $p = 0.0069$), high *TrkA* expression ($p = 0.002$), a single copy of *MYCN* ($p < 0.00005$), tumors found by mass screening ($p = 0.0042$), nonadrenal origin ($p = 0.0042$) and good prognosis ($p = 0.023$). The log-rank test showed that high expression of *hTTL* was an indicator of favorable prognosis ($p = 0.026$). Immunohistochemical analysis using specific antibodies generated by us demonstrated that tyrosinated tubulin (Tyr-tubulin), detyrosinated tubulin (Glu-tubulin) and *hTTL* as well as Δ2-tubulin were positive in favorable tumors, whereas only Δ2-tubulin was positive in the tumors with *MYCN* amplification. In an RTBM1 neuroblastoma cell line, hTTL was increased after treating the cells with bone morphogenetic protein 2 (BMP2) or all-trans retinoic acid (RA), which induced neuronal differentiation. These results suggest that the deregulated tubulin tyrosination/detyrosination cycle caused by decreased expression of hTTL is associated with inhibition of neuronal differentiation and enhancement of cell growth in the primary neuroblastomas with poor outcome.

Key words: *tubulin tyrosine ligase; tubulin tyrosination; neuroblastoma; neuronal differentiation; prognostic factor*

Tubulin is one of the most important molecular components that regulate cytoskeletal structure relating to cell motility, cell division, differentiation, invasion and metastasis in cancer. However, functional modification of tubulin protein has still been elusive. Tubulin is subjected to several types of evolutionarily conserved posttranslational modification that includes tyrosination/detyrosination, acetylation, phosophorylation, palmitoylation, polyglutamylation and polyglycylation.[1–4] The discovery of tyrosination cycle stems from the serial observations that the addition of radiolabeled tyrosine to a rat brain cytosolic extract leads to tyrosination of the COOH terminus of a single endogenous protein, α-tubulin, by a translation-independent mechanism.[5–7] Posttranslational incorporation of tyrosine into the tubulin has also been shown to occur *in vivo*.[8–10] The cycle of tyrosination/detyrosination is evolutionarily conserved[11–13] and is regulated by both tubulin tyrosine ligase (TTL) and carboxypeptidase, the gene of which has not yet been identified (Fig. 1). Microtubule dynamics is also an important factor. TTL protein was first purified by immunoaffinity chromatography from the lysates of bovine and porcine brains and was extensively characterized by protein sequencing.[14] Recently, rat *TTL* cDNA has also been isolated.[15] Interestingly, in 1991, Paturle-Lafanechere *et al.*[16] identified a nontyrosinatable variant of tubulin that lacked 2 amino acid residues, glutamic acid and tyrosine, at the COOH terminus (Δ2-tubulin). Δ2-tubulin was found to accumulate in mature neurons and in stable microtubule assemblies in cells.[17,18] In some tumors, it also accumulated in the cellular cytoplasm in association with decreased levels of TTL, suggesting that the amount of Δ2-tubulin and TTL expression level in tumor cells are important to define the malignant grade of cancer.[19] However, pathophysiologic significance of the tyrosination/detyrosination cycle in normal and cancer cells still remains unclear.

Neuroblastoma (NBL) is one of the most common childhood solid tumors and has distinct biologic characteristics in different prognostic subgroups. For example, NBL in patients under 1 year of age usually regresses spontaneously, whereas that in patients over 1 year of age often grows aggressively and eventually kills the patient. To understand the molecular mechanism of distinct biology and tumorigenesis of NBL, we have previously performed a comprehensive approach to unveil the gene expression profiles among the NBL subsets.[20,21] We constructed the subset-specific oligo-capping cDNA libraries from the primary NBL tissues with favorable (stage 1, high expression of *TrkA* and a single copy of *MYCN*) and unfavorable (stage 3 or 4, decreased expression of *TrkA* and *MYCN* amplification) characteristics and randomly cloned 4,654 cDNAs. After adding the cDNAs obtained from the stage 4s NBL cDNA library to our NBL gene collection, we made an in-house cDNA microarray carrying 5,340 genes proper to NBL. The comprehensive analysis of 136 NBLs using the microar-

Abbreviations: BMP2, bone morphogenetic protein 2; DMEM, Dulbecco's modified Eagle's medium; ECL, enhanced chemiluminescence; FBS, fetal bovine serum; hTTL, human tubulin tyrosine ligase; NBL, neuroblastoma; RA, retinoic acid; TCP, tubulin carboxypeptidase; TTL, tubulin tyrosine ligase.

Grant sponsor: Grant-in-Aid for Scientific Research and for Scientific Research on Priority Areas, Medical Genome Science from the Ministry of Education, Science, Sports and Culture, Japan; Grant sponsor: Hisamitsu Pharmaceutical Co. Inc.

*Correspondence to: Division of Biochemistry, Chiba Cancer Center Research Institute, 666-2 Nitona, Chuoh-ku, Chiba 260-8717, Japan. Fax: +81-43-265-4459. *E-mail:* akiranak@chiba-ccri.chuo.chiba.jp

Received 27 January 2004; Accepted 15 April 2004

DOI 10.1002/ijc.20431
Published online 23 June 2004 in Wiley InterScience (www.interscience.wiley.com).

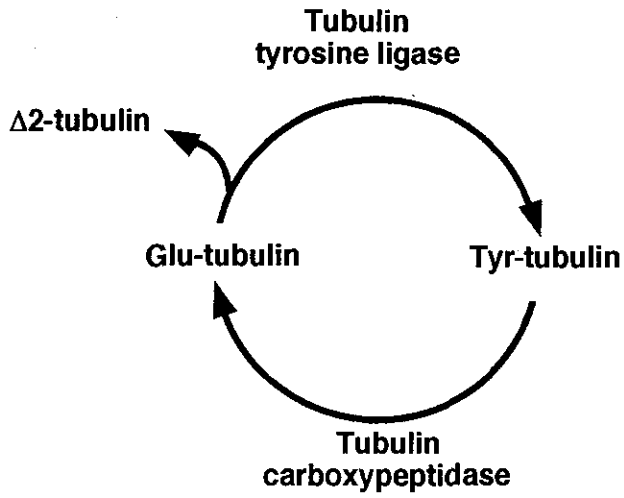

FIGURE 1 – The tyrosination/detyrosination cycle catalyzed by tubulin tyrosine ligase and tubulin carboxypeptidase.

ray showed that many genes that are related to the cytoskeletal components, including α-tubulin, had prognostic significance (data not shown).

In the present study, we have cloned for the first time the human ortholog of TTL (*hTTL*) from both the NBL and a fetal brain cDNA libraries. The analysis using 74 primary NBLs shows that expression of *hTTL* mRNA is significantly lower in unfavorable NBLs than in favorable tumors. The examination using specific antibodies raised against hTTL, Tyr-tubulin, Glu-tubulin and Δ2-tubulin demonstrates that hTTL is increased during induction of neuronal differentiation of cultured NBL cells treated with BMP2 or RA. The immunohistochemical study shows that hTTL, Tyr-tubulin, Glu-tubulin and Δ2-tubulin are positive in favorable NBLs, whereas only Δ2-tubulin is positive in aggressive NBLs with *MYCN* amplification. These suggested that the tyrosination/detyrosination cycle of α-tubulin is active in NBLs with high potential to differentiate or undergo apoptosis, while it is disregulated by downregulation of hTTL in *MYCN*-amplified NBLs, resulting in accumulation of Δ2-tubulin.

MATERIAL AND METHODS

Tumor specimen

Fresh frozen tumor tissues obtained by surgery or biopsy were sent to the Division of Biochemistry, Chiba Cancer Center Research Institute, from various hospitals in Japan with informed consent. Ninety tumors examined in this study were staged according to the International Neuroblastoma Staging System (INSS).[22] The number of tumors subjected to quantitative real-time RT-PCR were 24 in stage 1, 11 in stage 2, 5 in stage 4s, 10 in stage 3 and 24 in stage 4. The patients were treated according to the protocols previously described.[23] Biologic information on each tumor, including *MYCN* gene copy number, *TrkA* gene expression and DNA ploidy, was analyzed in our laboratory as described previously.[24]

Cell culture and transfection

COS7 and HEK293T cells were maintained in Dulbecco's modified Eagle's medium (DMEM) supplemented with 10% heat-inactivated fetal bovine serum (FBS; Life Technologies, Gaithersburg, MD) and penicillin (100 IU/ml)/streptomycin (100 μg/ml). Human neuroblastoma RTBM1 cells were grown in RPMI-1640 medium containing 10% heat-inactivated FBS and antibiotic mixture. Cultures were maintained at 37°C in a water-saturated atmosphere of 5% CO_2 in air. Transient transfection was performed by LipofectAMINE 2000 transfection reagent (Invitrogen, Carlsbad, CA) according to the manufacturer's instructions. In brief, cells were seeded in tissue culture plates to achieve 50% confluence. Twenty-four hours later, cells were transfected by using a mixture of the expression plasmids and LipofectAMINE 2000 transfection reagent in DMEM without serum. Forty-eight hours after transfection, cells were collected and analyzed by Western blotting. For neurite extension assays, RTBM1 cells were treated either with recombinant human BMP2 (Yamanouchi Pharmaceutical, Tokyo, Japan) or with RA at a final concentration of 1 nM or 5 μM, respectively.

RNA isolation and semiquantitative RT-PCR

Total RNA was prepared from neuroblastoma tissues according to the AGPC method.[25] Five micrograms of total RNA were subjected to the synthesis of the first-strand cDNA with $pd(N)_6$ random hexamer (Takara Shuzo, Otsu, Japan) and a Superscript II reverse transcriptase (Invitrogen) at 42°C for 90 min. The resultant cDNA was diluted to be a 1:20 solution and was amplified in a final volume of 10 μl of reaction mixture containing 100 μM of each deoxynucleoside triphosphate, 1 × PCR buffer, 1 μM of each primer and 0.2 U of *r*Taq DNA polymerase (Takara Bio, Ohtsu, Japan). The following primers were used: *hTTL*, 5′-CAGCTCTTCGGCTTTGACTT-3′ (sense) and 5′-GCTGTGGGCTGGATAAAGAG-3′ (antisense); human *GAPDH*, 5′-ACCTGACCTGCCGTCTAGAA-3′ (sense) and 5′-TCC ACCACCCTGTTGCTGTA-3′ (antisense). PCR templates were standardized by its *GAPDH* expression before performing semiquantitative PCR experiment. The PCR-amplified products were separated by electrophoresis on a 1.5% agarose gel and visualized by ethidium bromide poststaining.

Quantitative real-time RT-PCR

cDNA was prepared by the same method as in the semiquantitative RT-PCR and 2 μl of the 40-fold dilution was used for each PCR reaction. Primers and TaqMan probes for *hTTL* were designed using the primer design software Primer Express (Perkin-Elmer Applied Biosystems, Foster City, CA). The primer sequences for *hTTL* are 5′-AAGGAACTGCCTCCTGAGC-3′ and 5′-TCAATGAGCCAC ACCTTCA-3′. The probe sequence for *TTL* is 5′-FAM-ATTAGC ACCAAGCACCTCCCTTACCAGAGC-TAMRA-3′. PCR was carried out with the ABI Prism 7700 Sequence Detection System (Perkin-Elmer Applied Biosystems). Two μl of cDNA was amplified in a final volume of 25 μl containing 1 × TaqMan mixture, 300 nM each primer and 200 nM TaqMan probe. The thermal cycling condition was as follows: 50 cycles of a 2-step PCR (95°C for 15 sec, 60°C for 1 min) after the initial activation of UNG followed by denaturation (50°C for 2 min, 95°C for 10 min). TaqMan *GAPDH* control reagent kit (Roche Molecular Biochemicals, Basel, Switzerland) was used for the amplification of *GAPDH* according to the manufacturer's instructions; all data were normalized using *GAPDH* expression. The experiments were performed in triplicate for each data point.

Generation of polyclonal anti-hTTL antibodies

The polyclonal anti-hTTL antibody was raised in rabbits against Cys-coupled synthetic peptides derived from hTTL (222-RTASEPY-HVDNFQDKTCHLTNH-243 and 244-CIQKEYSKNYGKYEE-GNE-261). The polyclonal anti-Tyr-tubulin, anti-Glu-tubulin and anti-Δ2-tubulin antibodies were raised in rabbits immunized with Cys-coupled synthetic peptides corresponding to their COOH termini (CEEEGEEY, CGEEEGEE and CEGEEEGE, respectively). Antibodies were purified by using peptide-coupled affinity columns and tested for their ability to identify the corresponding proteins by Western blots. The synthetic peptides and antibodies were generated by Protein Express (Chiba, Japan).

Construction of FLAG-tagged hTTL expression plasmid

The FLAG-tagged hTTL expression plasmid was generated by PCR amplification using the cDNA library derived from human fetal brain (Stratagene, La Jolla, CA) and an *hTTL* cDNA that lacked the 5′-portion encoding the NH_2 terminal region of hTTL as templates. The forward and reverse primers used were 5′-TAAATAGTCGACGATATC**ATGGACTACAAGGACGAC**

GACGACAAGTACACCTTCGTGGTACGCGATGAGAACAGC AGCGTCTACGCCGAGGTCTCCCGGCTGCTCCTCGCCA-3′ (sequence encoding FLAG epitope tag is in boldface, and *Eco*RV recognition site is underlined) and 5′-TACATGTCGACGCGG CCGCTCACAGCTTGAT GAA-3′ (*Not*I restriction site is underlined). The resulting PCR product was gel-purified, digested with *Eco*RV and *Not*I, inserted into identical restriction sites of a mammalian expression plasmid pIRESpuro2 (Clontech Laboratories, Palo Alto, CA) and its nucleotide sequence was verified by automated dideoxy terminator cycle sequencing.

Western blot analysis

Cells were washed in ice-cold phosphate-buffered saline (PBS), collected by centrifugation and lysed in 1 × sample buffer. Equal amounts of whole-cell lysates were fractionated by SDS-polyacrylamide gel electrophoresis (SDS-PAGE), and electrophoretically transferred onto a polyvinylidene difluoride (PVDF) membrane filter (Immobilon-P; Millipore, Billerica, MA). The filter was then blocked with Tris-buffered saline (TBS) containing 5% nonfat dry milk at room temperature for 1 hr and subsequently incubated for 1 hr with the antibodies against hTTL, Tyr-tubulin, Glu-tubulin, Δ2-tubulin, α-tubulin (5H1; PharMingen, San Diego, CA) and actin (20-33; Sigma Chemical, St. Louis, MO). The filter was further incubated with horseradish peroxidase-conjugated mouse or rabbit IgG secondary antibody (Cell Signaling Technologies, Beverly, MA). Immunoreactivity was detected using the enhanced chemiluminescence system (ECL; Amersham Pharmacia Biotechnology, Uppsala, Sweden) according to the manufacturer's instructions. The films were exposed at multiple time points to ensure that the images were not saturated.

Immunohistochemistry

Immunohistochemical stainings with antibodies against hTTL (1:100), Tyr-tubulin (1:100), Glu-tubulin (1:100) and Δ2-tubulin (1:100) were performed on 10 human neuroblastoma tumors selected from the surgical pathology file at the Department of Pathology, Aichi Medical University, based on the results of histopathology evaluation[26] and *MYCN* status. Also performed were immunostainings with antibodies against TrkA (1:40, 763; Santa Cruz Biotechnology, Santa Cruz, CA), CD56 (1B6; Novocastra Laboratories, Peterborough, U.K.) and Ki-67 (1:200, MIB-1; Dako, Kyoto, Japan) on the same tumor tissues. All of those tumor samples were obtained prior to chemotherapy and irradiation therapy and included 6 favorable histology cases with nonamplified *MYCN* (FH&NA) and 4 unfavorable histology cases with amplified *MYCN* (UH&A). Among the neuroblastoma cases, tumors in the FH&NA subset were reported to be the most favorable biologically and clinically. In contrast, tumors in the UH&A subset are known to be the most aggressive with the poorest clinical outcome.[27] Four μm thick sections from the formalin-fixed and paraffin-embedded tissue samples were deparaffinized and microwaved for 3 × 5 min in Na-citrate buffer (pH 6.0) for antigen retrieval. The slides were first immersed in 0.3% hydrogen peroxide in methanol for 20 min and then in 10% normal goat serum for 30 min. The primary antibodies were then applied at 4°C overnight, followed by a standard staining procedure using the Vectastain ABC kit (Vector Laboratories, Burlingame, CA). Sections were counterstained with hematoxylin for light microscopic review and evaluation. hTTL, Tyr-tubulin, Glu-tubulin and Δ2-tubulin were always positively detected in the cytoplasm and neuritic processes of normal ganglion cells in the separate positive control sections as well as in the test sections as built-in control, whenever available. As for the negative controls of hTTL, Tyr-tubulin, Glu-tubulin, Δ2-tubulin and TrkA stainings, normal rabbit immunoglobulins (1:500 dilution, Vector Laboratories) were applied as the primary antibody. As for the negative controls of CD56 and Ki-67 stainings, we followed the staining procedure without the primary antibodies.

Statistical analysis

Student's *t*-tests were used to explore possible associations between *hTTL* expression and other factors, such as age. Since the values of the *hTTL* expression were skewed, a log transformation was used to achieve the normality when using *t*-test and Cox regression. The distinction between high and low levels of *hTTL* was based on the median value (*low*, *hTTL* < 95 e.u.; high, *hTTL* > 95 e.u.), regardless of tumor stage, *MYCN* copy number, or survival. Kaplan-Meier survival curves were calculated, and survival distributions were compared using the log-rank test. Cox regression models were used to explore associations between *hTTL* expression, age, *MYCN* amplification, mass screening, origin and survival. Statistical significance was declared if the *p*-value was < 0.05. Statistical analysis was performed using Stata 7.0. (Stata, College Station, TX).

RESULTS

Cloning and expression of hTTL *gene*

We have previously constructed oligo-capping cDNA libraries from 3 fresh human NBL tissues (stages 1 and 2, high *TrkA* expression and a single copy of *MYCN*), which were gradually undergoing spontaneous regression probably due to neuronal apoptosis.[20] Screening of 1,152 novel genes by reverse transcriptase (RT)-PCR revealed that 194 genes were expressed differentially between NBLs with favorable prognosis and those with unfavorable outcome. Among them, we detected a partial cDNA sequence (*Nbla00660*) corresponding to the human ortholog of *tubulin tyrosine ligase* (*hTTL*) gene. We then cloned the full-length *hTTL* cDNA using both conventional phage library screening and genome sequence-based RT-PCR procedure. The *hTTL* gene was mapped to chromosome 2q13 and consisted of 7 exons (Fig. 2*a*) with 377 predicted amino acids (Genbank/DDBJ accession number AB071393; Fig. 2*b*). Comparison of the deduced amino acid sequence of human *TTL* cDNA with those of mouse, rat, pig and cow showed identity by 94%, 94%, 93% and 94%, respectively. *hTTL* was ubiquitously expressed in various human tissues including heart, kidney, lung, colon, thymus, spleen, mammary gland, testis, prostate, brain, cerebellum, liver, fetal brain, fetal liver, adrenal gland and skeletal muscle (Fig. 2*c*). However, it was rather preferentially expressed in adult and fetal brains and lung.

Specific antibodies and catalytic activity of hTTL

To study the role of hTTL and the tyrosination/detyrosination cycle regulated by TTL in neuroblastoma, we generated specific antibodies against human Tyr-tubulin, Glu-tubulin and Δ2-tubulin based on the previous reports.[16,18,28] The PVDF membranes spotted with equal amount (1 μg) of synthetic peptides corresponding to COOH terminal 7 amino acid residues of Tyr-tubulin (CEEEGEEY), Glu-tubulin (CGEEEGEE) and Δ2-tubulin (CEGEEEGE) were immunoblotted with rabbit anti-Tyr-tubulin antibody (Fig. 3*a*, top), anti-Glu-tubulin antibody (Fig. 3*a*, middle) and anti-Δ2-tubulin antibody (Fig. 3*a*, bottom), respectively. There were no crossreactivities among them, suggesting that those 3 antibodies were highly specific to each form of tubulin. To confirm the catalytic activity of hTTL encoded by the gene we cloned, we transfected the HEK293T cells with various amount of *hTTL* expression construct. Increased levels of hTTL in those cells induced tyrosination of tubulin in dose-dependent manner, while the level of endogenous Glu-tubulin was decreased (Fig. 3*c*). These results showed that hTTL protein encoded by the gene we cloned has its catalytic activity.

Upregulation of hTTL expression during neuronal differentiation

BMP2 has been characterized as a neurotrophic factor.[29] Recently, Nakamura *et al.*[30] have reported that RTBM1, a human neuroblastoma cell line, is responsive to both BMP2 and RA by extending neurites. By using this system, we examined whether the expression levels of hTTL change during induction of neuronal differentiation. As shown in Figure 4, the treatment of RTBM1

a

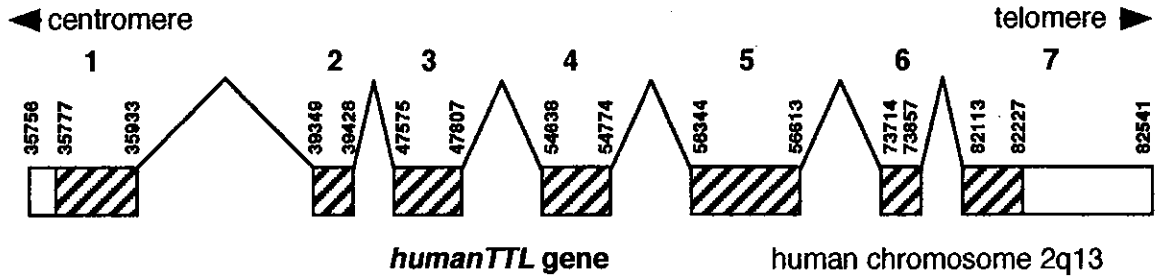

b

```
humanTTL  MYTFVVRDENSSVYAEVSRLLLATGHWKRLRRDNPRFNLMLGERNRLPFGRLGHEPGLVQLVNYYRGADKLCRKAS 76
mouseTTL  MYTFVVRDENSSVYAEVSRLLLATGYWKRLRRDNPRFNLMLGERNRLPFGRLGHEPGLAQLVNYYRGADKLCRKAS 76
ratTTL    MYTFVVRQENSSVYAEVSRLLLATGYWKRLRRDNPRFNLMLGGRNRLPFGRLGHEPGLAQLVNYYRGADKLCRKAS 76
pigTTL    MYTFVVRDENSSVYAEVSRLLLATGHWKRLRRDNPRFNLMLGERNRLPFGRLGHEPGLMQLVNYYRGADKLCRKAS 76
cowTTL    MYTFVVRDENSSVYAEVSRLLLATGHWKRLRRDNPRFNLMLGERNRLPFGRLGHEPGLMQLVNYYRGADKLCRKAS 76
          ******* ***************** ***************** ***************** *****************

humanTTL  LVKLIKTSPELAESCTWFPESYVIYPTNLKTPVAPAQNGIQPPISNSRTDEREFFLASYNRKKEDGEGNVWIAKSS 152
mouseTTL  LVKLVKTSPELSESCSWFPESYVIYPTNLKTPVAPAQNGIQLPVSNSRTDEREFFLASYNRKKEDGEGNVWIAKSS 152
ratTTL    LVKLVKTSPELSESCSWFPESYVIHPTNLKTPVAPAQNGIQLPVSNSRTDEREFFLASYNRKKEDGEGNVWIAKSS 152
pigTTL    LVKLIKTSPELAESCTWFPESYVIYPTNLKTPVAPAQNGIHPPIHSSRTDEREFFLTSYNKKKEDGEGNVWIAKSS 152
cowTTL    LVKLIKTSPELAESCTWFPESYVIYPTNLKTPVAPAQDGIHPPLHSSRTDEREFFLASYNRKKEEGEGNVWIAKSS 152
          **** ****** *** ******** ************ **  *   ********** *** *** ************

humanTTL  AGAKGEGILISSEASELLDFIDNQGQVHVIQKYLEHPLLLEPGHRKFDIRSWVLVDHQYNIYLYREGVLRTASEPY 228
mouseTTL  AGAKGEGILISSEASELLDFIDSQGQVHVIQKYLERPLLLEPGHRKFDIRSWVLVDHQYNIYLYREGVLRTASEPY 228
ratTTL    AGAKGEGILISSEASELLDFIDNQGQVHVIQKYLEHPLLLEPGHRKFDIRSWVLVDHQYNIYLYREGVLRTASEPY 228
pigTTL    AGAKGEGILISSEATELLDFIDNQGQVHVIQKYLERPLLLEPGHRKFDIRSWVLVDHQYNIYLYREGVLRTASEPY 228
cowTTL    AGAKGEGILISSDATELLDFIDNQGQVHVIQKYLERPLLLEPGHRKFDIRSWVLVDHQFNIYLYREGVLRTASEPY 228
          ************ * ******* ************ ********************** *****************

humanTTL  HVDNFQDKTCHLTNHCIQKEYSKNYGKYEEGNEMFFKEFNQYLTSALNITLESSILLQIKHIIRNCLLSVEPAIST 304
mouseTTL  HVDNFQDKTCHLTNHCIQKEYSKNYGKYEEGNEMFFEEFNQYLTSALNITLESSILLQIKHIIRSCLMSVEPAIST 304
ratTTL    HVDNFQDKTCHLTNHCIQKEYSKNYGKYEEGNEMFFEEFNQYLTSALNITLENSILLQIKHIIRSCLMSVEPAIST 304
pigTTL    HTDNFQDKTCHLTNHCIQKEYSKNYGKYEEGNEMFFEEFNQYLTSALNITLESSILLQIKHIIRSCLLSVEPAIST 304
cowTTL    HMDNFQDKTCHLTNHCIQKEYSKNYGKYEEGNEMFFEAFNRYLTSALNITLESSILLQIKHIIRSCLMSVEPAIST 304
          * ********************************  ** *********** *********** ** ********

humanTTL  KHLPYQSFQLFGFDFMVDEELKVWLIEVNGAPACAQKLYAELCQGIVDIAISSVFPPPDVEQPQTQP--AAFIKL  377
mouseTTL  KHLPYQSFQLLGFDFMVDEELKVWLIEVNGAPACAQKLYAELCQGIVDIAISSVFPPPDTEQVPQQP--AAFVKL  377
ratTTL    KHLPYQSFQLLGFDFMVDEELKVWLIEVNGAPACAQKLYAELCQGIVDIAISSVFPPPDTEQVPQQP--AAFMKL  377
pigTTL    RHLPYQSFQLFGFDFMVDEDLKVWLIEVNGAPACAQKLYAELCQGIVDIAIASVFPPPDAEQQQQQPPPAAFIKL  379
cowTTL    KHLPYQSFQLFGFDFMVDEELKVWLIEVNGAPACAQKLYAELCQGIVDIAIASVFPPPDAEQQPPQP--ATFIKL  377
          ********* ******** ******************************** ******* **   **  * * **
```

c

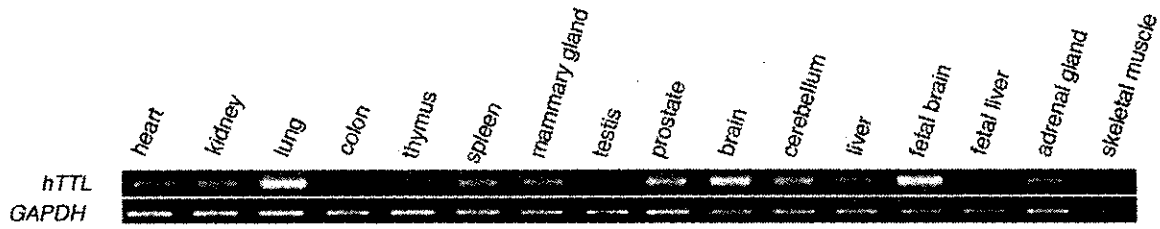

FIGURE 2